2015

Examining the Sensitivity of Surface Chlorophyll to Upwelling Events of Variable Frequency in the California Current System

John Thomas Bartlett
University of South Carolina - Columbia

EXAMINING THE SENSITIVITY OF SURFACE CHLOROPHYLL TO UPWELLING EVENTS OF VARIABLE FREQUENCY IN THE CALIFORNIA CURRENT SYSTEM

by

John Thomas Bartlett

Bachelor of Science
North Carolina State University, 2013

Submitted in Partial Fulfillment of the Requirements

For the Degree of Master of Science in

Marine Science

College of Arts and Sciences

University of South Carolina

2015

Accepted by:

Ryan Rykaczewski, Director of Thesis

George Voulgaris, Reader

Venkat Lakshmi, Reader

Lacy Ford, Vice Provost and Dean of Graduate Studies

DEDICATION

Roses are red,

Violets are blue,

Jenna Leigh,

This work is dedicated to you!

ACKNOWLEDGEMENTS

First and foremost, this work would have never been accomplished without Jesus Christ my Savior, who provided me the fortitude to overcome the many obstacles of graduate school and ultimately, succeed in His honor. I would like to thank Dr. Ryan Rykaczewski for accepting me into his lab and providing the guidance needed to shape me into a more critical scientist. Thanks to Dr. George Voulgaris and Dr. Venkat Lakshmi for reviewing and critiquing my thesis work. A special thanks to Dr. Ron Benner, Dr. Claudia Benitez-Nelson, and the Marine Science Program for the financial support and many opportunities provided throughout my graduate school experience. Also, I want to convey my deepest appreciation to my beautiful fiancée, Jenna, for her boundless love and encouragement throughout this process. To my parents (step-parents), John (Laura) and Carolyn (Charles), and my brother, Chad, who provided me with an immense amount of emotional support. Thanks to my second family, Ms. Angie, Lucas, Jayme, Adrian, Rosie, Chandler, and Chachi. Also, thank you to my two roommates Toni and Pepper. Additionally, I would like to thank my lab mates Steven Vega, Brian Grieve, Camaron George, and Clifford Felton as well as my fellow classmates. Finally, I would like to acknowledge the Geophysical Fluid Dynamics Laboratory for providing the CM2.6 model data, which allowed me to conduct this study.

ABSTRACT

Eastern Boundary Upwelling Systems (EBUS) spatially encompass approximately 1% of the ocean surface area, but are responsible for nearly 20% of global fisheries production. This significant biological production is primarily attributed to the nutrient-rich waters brought to the euphotic zone through a physical process called upwelling. In an attempt to understand the various physical and biological processes occurring on a wide range of temporal and spatial scales, the California Current System (CCS), one of the major EBUS, has been subject to a multitude of scientific studies over the past several decades. Recent modeling enhancements have enabled researchers to investigate mesoscale processes contributing to physical and biological variability within the CCS. This information could be used to improve our understanding of plankton dynamics and ultimately, be applied to higher trophic levels and coastal fisheries management.

The primary focus of this study was to investigate whether high-frequency (3 – 7 days) wind events generate a positive response in surface chlorophyll-a (chl-a) within regions of the CCS. The high-frequency wind events were hypothesized to be insufficient to generate enough upwelling and subsequent lift in the nutricline to produce a significant response in surface chl-a concentrations. Rather, I expected that low-frequency (7 – 30 days) upwelling-favorable wind events would raise the nutricline for a period long enough to sustain a phytoplankton bloom. Utilizing high-resolution climate model data, a frequency analysis was performed by conducting a correlation between

chl-a concentrations and meridional wind stress (τ_y) events at lagged intervals. High-frequency τ_y events are found to have a minimal impact on chl-a concentrations throughout the CCS. At low frequencies, chl-a concentrations were shown to have a positive response to τ_y events within 100km of the CCS coastline. These results imply that high-frequency upwelling events have little to no immediate impact on the chl-a concentrations. However, the low-frequency τ_y events appear to persist long enough to generate a response in surface chl-a and positively impact productivity within the CCS.

TABLE OF CONTENTS

LIST OF FIGURES

CHAPTER 1

EXAMINING THE SENSITIVITY OF SURFACE CHLOROPHYLL TO UPWELLING EVENTS OF VARIABLE FREQUENCY IN THE CALIFORNIA CURRENT SYSTEM

1.1 INTRODUCTION

Major Eastern Boundary Upwelling Systems (EBUS) exist within four key regions across the globe: (1) the California Current in the Northeast Pacific Ocean, (2) the Humboldt Current in the Southeast Pacific Ocean, (3) the Canary Current in the Northeast Atlantic Ocean, and (4) the Benguela Current in the Southeast Atlantic Ocean. These regions only spatially encompass 1% of the ocean surface, but are responsible for nearly 20% of global fisheries production [*Mann*, 2000]. The significant biological production within these regions has been primarily attributed to a physical phenomenon called coastal upwelling. Alongshore, equatorward winds force the surface water offshore, away from the coastline, through the process of Ekman transport [*Checkley and Barth*, 2009; *Huyer*, 1983]. This in-turn forces relatively cold, nutrient-rich subsurface waters toward the surface, also known as upwelling. Thermoclines and nutriclines that shoal into the euphotic zone along the coast are common features of EBUS during upwelling periods [*Bakun et al.*, 2010]. The opposite effect occurs during wind events that are primarily poleward; surface waters are transported toward the coastline, which forces relatively warm, nutrient poor surface waters to sink and downwell [*Chelton et al.*, 1982]. In the California Current System (CCS), these coastal upwelling events can cause localized changes to the physical (Figure 1.1a) and biological (Figure 1.1b) properties of the surface water along the coastline. Upwelling processes in all EBUS are influenced by both synoptic and mesoscale atmospheric-oceanic coupled variability in addition to coastal orography [*Huyer*, 1983]. These processes are typically at their strongest during late spring and early summer, when the wind stress is primarily equatorward. Throughout the summer months (July-September), thermal stratification strengthens due

to the increased light availability and the depth of the mixed layer shoals [*Palacios et al.*, 2004]. The seasonal reversal of the meridional winds during the winter months (December and February) induces either downwelling (common in the poleward portions of EBUS) or low upwelling rates (common in the equatorward portions of EBUS). Ultimately, the magnitude, direction, and spatial structure of the surface winds within the California Current System (CCS) alter the local ecology [*Bakun*, 1990; *Rykaczewski and Checkley*, 2008].

These nutrient-rich, upwelled waters can positively influence primary productivity as well as indirectly increase productivity in the higher trophic levels within the EBUS food chains. Within the euphotic zone, the ocean layer that light penetrates or about the upper 200m, the first trophic level is composed of phytoplankton. Phytoplankton are microorganisms that utilize light energy to synthesize organic matter through photosynthesis. In addition to light concentration, both water temperature and nutrient availability can impact phytoplankton growth. The primary nutrients required by phytoplankton are nitrate, phosphate, and iron, and diminished growth rates can occur when concentrations of these nutrients are limiting [*Miller and Wheeler*, 2012]. Water temperature impacts growth rates and reaction rates and is linked with nutrient availability. Although the relative impact will vary between the different species of phytoplankton, growth rates are typically greater at water temperatures above 10°C [*Miller and Wheeler*, 2012].

Due to the growing concern regarding the impacts of climate change on fisheries productivity, the ecological consequences of variable surface winds within these EBUS have been explored at decadal to seasonal timescales. *McGowan et al.* [2003] used a 50-

year time series to assess the decadal oscillations and 1977-regime shift within the CCS. This decadal transition to a low-nutrient regime along the coast is hypothesized to be a result of the intensification of the Aleutian Low pressure system over the North Pacific Ocean [*Chavez et al.,* 2003]. This intensification increased coastal stratification, dampened coastal upwelling rates, and decreased horizontal advection of the nutrient-rich waters from the north. Also, model estimations have indicated that decreases in plankton concentrations may be a response to long-term (1949-2000) warming trends [*Di Lorenzo et al.*, 2005].

Environmental phenomena on interannual scales have also been studied extensively within the CCS, such as the El Niño-Southern Oscillation (ENSO). The extreme El Niño event of 1997-1998 for example, led to very low upwelling rates and significant upper ocean stratification, which was found to negatively impact the primary and secondary production within the CCS [*Bograd and Lynn*, 2001]. Conversely, the subsequent La Niña event of 1999 initiated strong, sustained upwelling throughout the CCS. As a result, coastal SSTs were about 3°C lower than the seasonal average and increased surface chl-a concentrations over a broad region extending to further than 50km offshore [*Schwing et al.*, 1999]. A seasonal correlation has also been found between the chl-a responses within the four EBUS and wind-induced upwelling [*Thomas et al.*, 1994; *Demarcq*, 2009]. *Garcia-Reyes and Largier* [2012] conducted an analysis of the differences between the geostrophically-derived wind stress used within the Bakun Upwelling Index (UI) calculation and observed wind stress. Both datasets captured three distinct seasonal periods: Upwelling Season (April-June), Relaxation Season (July-September), and Storm Season (December-February). However, the coarse, 3°x3°

resolution of the atmospheric model used to estimate the geostrophic winds could not account for the small-scale atmospheric fluctuations (i.e. frontal passages) or topographic influences (i.e. capes and points) [*Garcia-Reyes and Largier*, 2010; *Garcia-Reyes and Largier*, 2012].

Modeling studies have been used for many years to quantify both physical and biological processes in the CCS [*Di Lorenzo et al.*, 2004; *Spitz et al.*, 2003]. *Botsford et al.* [2003] and *Wroblewski et al.* [1989] used idealized model studies to investigate the optimal surface wind conditions for zooplankton and larval fish. These studies indicated that wind pulses must be upwelling-favorable over durations long enough for nutricline shoaling to reach into the euphotic zone; however, realistic models are required to quantify and examine the physical and biological processes that occur. Recent improvements in modeling resolution have provided finer, three-dimensional resolutions than previous models and have enabled scientists to research smaller coastal features. The Geophysical Fluid Dynamics Laboratory (GFDL) has been developing atmosphere-ocean coupled climate models (CM) with interactive biogeochemical components to research the impacts of global climate change on marine ecosystems. Both model dynamics and resolution have been improved with each new model version (i.e. CM2.1, CM2.5, CM2.6). The improvement in resolution from CM2.1 to CM2.5 included an increase in atmospheric resolution from 200km to about 50km and in oceanic resolution from 100km to about 28km. This enhancement allows CM2.5 to better capture such seasonal events as ITCZ migration, ENSO events, precipitation patterns, and river discharge [*Delworth et al.*, 2012]. Also, both CM2.5 and the new CM2.6 have the capacity to resolve mesoscale eddy formation, with the CM2.6 having an enhanced 1/10°

(about 10km) grid scale resolution in the ocean [*Wintson et al.*, 2014]. In addition to representing the physical circulation of the atmosphere and ocean, CM2.6 includes an ecosystem model called the Carbon, Ocean Biogeochemistry and Lower Trophics (COBALT) model. COBALT uses complex nutrient and food web dynamics to best represent nutrient cycling, carbon biogeochemistry, and dynamics of a simplified planktonic food web within the ocean [*Stock et al.*, 2014], which is further described in Section 1.3.1.

Past research studies have noted that high-frequency events exist within the CCS, but the influence of these events on the local surface biology is relatively unknown [*Huyer*, 1983]. *Michaelsen et al.* [1988] used a 30-month time series of pigment measurements from the Coastal Zone Color Scanner (CZCS) to analyze the temporal variability of phytoplankton within the CCS. The results supported previous assessments noting a dominant seasonal cycle within the CCS, but a high-frequency atmospheric signal of about five to six days was also evident, which was explained by the passages of mid-latitude cyclones [*Bane et al.*, 2007]. Additionally, *Bane et al.* [2007] found that the atmospheric jet stream has intraseasonal (10 – 100 days) oscillations that impact the coastal wind stress within the CCS. Atmospheric pressure anomalies have also been shown to impact the CCS at time scales on the order of a week to a month [*Legaard and Thomas,* 2006]. Sparse ship observations [*Goodman et al.*, 1984] and simple model studies [*Botsford et al.*, 2003] have observed phytoplankton blooms to occur on weekly time scales in response to an increased flux of nutrients. Persistent upwelling-favorable wind events over multiple day periods have been shown to induce low sea surface heights and bring dense waters to the surface along the CCS coastline [*Strub et al.*, 1987].

Increased temporal and spatially robust satellite-derived and model-estimated datasets have allowed recent research to focus on mesoscale features within the CCS and the other EBUSs. High-resolution scatterometers (surface wind) and radiometers (SST) have been used to identify high-frequency upwelling events of three to seven days within the Benguela Current System [*Desbiolles et al.*, 2014]. *Botsford et al.* [2006] utilized a mixed-layer conveyor model and determined that the wind speed and direction over the continental shelf must be relatively static for a minimum duration of three days to have an ecological significance, which was approximated as the amount of time considered necessary for phytoplankton to complete nutrient uptake [*Botsford et al.*, 2006]. Thus, high-frequency (3 – 7 days) and low-frequency (7 – 30 days) wind events have been shown to have a direct impact on ocean physics and as a result, have a potential influence on the surface biology.

The CCS has a linear coastline north of Cape Blanco with scalloped coastline and headlands present between Cape Blanco and Point Conception [*Kahru and Mitchell*, 2001]. Due to the differences in atmospheric-ocean dynamics and orography, which affects the wind speed, wind direction, and the relative magnitude and timing of primary productivity, previous studies [*Strub et al.*, 1990; *Thomas et al.*, 2004] have analyzed the CCS in specific subsections: northern CCS (~41.5°N – 46.5°N), central CCS (~35.5°N – 41.5°N), and southern CCS (~30.5°N – 35.5°N). In addition to latitudinal dissimilarities within the CCS, physical and biological dynamics evolve differently with regard to distance from the coastline. Throughout the entire CCS, coastal upwelling occurs within a narrow band within about 25km of the coast [*Huyer*, 1983]. Between about 25km to 100km offshore, coastal plumes and filaments extend from the coastline toward the open

ocean [*Abbott and Zion*, 1987]. Further offshore, phytoplankton concentrations typically decrease from 100km to 300km offshore and even more drastically past 300km from the coastline [*Thomas et al.*, 1994; *Strub et al.*, 1990].

While upwelling variability at the decadal to seasonal time scales has been explored thoroughly, and high-frequency upwelling events have been shown to occur in EBUS, the ecological impact induced by high-frequency wind events has had minimal investigation. By furthering our current knowledge of the mesoscale phenomena and other physical forcings that impact the CCS, a more complete description of the drivers of biological variability may develop. This information could be used to improve our understanding of plankton bloom dynamics and ultimately, be applied to coastal fisheries management [*Di Lorenzo et al.*, 2004]. The primary focus of this study is to utilize high-resolution GFDL CM2.6 data to investigate whether high-frequency upwelling-favorable wind events generate a positive response in surface chl-a within regions of the CCS and if a relationship exists, to investigate its seasonality. It is **hypothesized** that high-frequency (3 – 7 days), upwelling-favorable wind events will not stimulate enough upwelling and nutrients to produce a significant relationship with surface chl-a concentrations. Rather, that low-frequency (7 – 30 days) upwelling-favorable wind events will raise the nutricline for a period long enough to sustain phytoplankton blooms. Furthermore, the relationship between chl-a and wind events will be more correlated during the summer months; due to the increased light availability (relative to winter months) and the amplified surface winds that could break down near-surface stratification, upwelled nutrients and that phytoplankton would be concentrated in the euphotic zone. The remaining portion of this thesis discussion will review characteristic physical and biological dynamics in the CCS

(Section 2), describe the model data, model assessment, and analytical methods used for this study (Section 3), convey the study results (Section 4), and discuss the study results and conclusions (Section 5).

1.2 STUDY REGION

1.2.1 The Physical and Biological Overview: Synoptic scale Influence

The CCS is a region where the dynamic coupling between the atmosphere and the ocean is robust. The Aleutian Low (AL) and the North Pacific High (NPH) pressure systems are the primary basin-scale atmospheric features that influence the dynamics in this region, as shown in Figure 1.1. Studies have shown that the positions of the AL and NPH alter the regional sea-surface height and near surface wind patterns seasonally [*Huyer*, 1983; *García-Reyes et al.*, 2013]. *Huyer* [1983] conveyed that the seasonal fluctuations in the surface environment were due to the seasonal shifts in the location and strength of these two pressure systems. Figure 1.2 displays the average wintertime sea-level pressure (SLP) in the North-central Pacific Ocean, and the signature of the AL is evident. Conversely, the NPH (AL) strengthens (weakens) during the summer months (Figure 1.2) in addition to continental SLP lowering [*Huyer*, 1983]. The average position of these pressure systems cause surface winds to be directed eastward across the central North Pacific, between the AL and NPH, until eventually diverging into a northward and southward flow due to the orographic influence of the coastline [*Huyer*, 1983; *Checkley and Barth*, 2009]. These surface winds circulating around the AL and NPH along the coastline influence the surface dynamics of the entire CCS [*Dorman and Winant*, 1995].

The direct atmosphere-ocean coupling impacts both surface and subsurface properties through Ekman transport. Ekman dynamics involve the interaction between

surface winds and the ocean surface. Due to the rotation of Earth and the Coriolis force, this frictional stress on the surface ocean initiates ripples and waves. In the Northern Hemisphere, the total movement of water within the Ekman layer is 90° to the right of the wind direction and is called Ekman transport. Along the CCS, where surface winds are moving toward the equator, the general transport of the subsurface waters is towards the west (offshore). The opposite occurs during poleward wind events; Ekman transport to the right of poleward-directed wind events cause water to pile up near the coastline and minimize upwelling [*Chelton et al.*, 1982; *Huyer*, 1983]. During an upwelling event, the thermocline and nutricline are forced upward, with upwelling velocities between 10 – 20 m d^{-1}, and force the movement of the cold, nutrient-rich waters toward the surface [*Bakun et al.*, 2010; *Checkley and Barth*, 2009; *McGowan et al.*, 2003]. Past research has demonstrated that a close relationship exists between the location of the thermocline and nutricline within the CCS [*McGowan et al.*, 2003; *Bograd and Lynn*, 2001]. Increased vertical stratification has also been hypothesized to reduce the response of nutricline shoaling to upwelling-favorable winds and plankton productivity [*Roemmich and McGowan*, 1995]. Although stratification can be induced by seasonal river discharge, the average stratification does not fluctuate significantly throughout the CCS [*Huyer*, 1983]. Seasonally, the thermocline depth is shallowest during February or March, while the maximum thermocline depth occurs after the substantial oceanic warming during the late summer months [*Palacios et al.*, 2004].

The importance of understanding this physical coupling between the atmosphere and ocean is often attributed to its significant influence on the ecosystem productivity. As previously mentioned, cold waters brought up into the euphotic zone through

upwelling are rich in inorganic nutrients [*McGowan et al.*, 2003; *Bograd and Lynn*, 2001]. Additionally, nutrients are also supplied by horizontal advection from the north to more southern portions of the CCS [*Chelton et al.* 1982]. Phytoplankton utilize these nutrients to synthesize of organic matter.

Both eukaryotic (i.e. diatoms, dinoflagellates) and prokaryotic (i.e. cyanobacteria) phytoplankton exist within the CCS. A couple common prokaryotes found in the CCS include *Synecoccus* and *Prochlorococcus* [*Collier and Palenik*, 2003]; and *Venrick* [2002] characterized key eukaryotes including *Chaetoceros spp.* (diatom) and *Ceratium spp.* (dinoflagellate). The unique aspect of the CCS is the presence of these larger, eukaryotic phytoplankton, which typically have a low abundance in the open ocean. These primary producers act as the base for a productive food web. Prominent zooplankton within the CCS include copepods, chaetognaths, and euphausiids [Checkley *and Barth*, 2009]. Many organisms further up the CCS food chain, such as pelagic fish, marine mammals, and sea birds [*Checkley and Barth*, 2009], are prevalent due to high phytoplankton and zooplankton productivity.

Seasonal fluctuations in physical dynamics influence the biological composition throughout the CCS. Diatoms dominate the northern region during periods of upwelling, but during relaxation and downwelling events smaller phytoplankton such as nanoflagellates and cyanobacteria dominate. The larger phytoplankton are grazed by mesozooplankton such as copepods (*Calanas spp.)* and krill (*Euphausia pacifica*), while the smaller phytoplankton are consumed by microzooplankton [*Kudela et al.*, 2008]. The seasonal fluctuations in plankton productivity also influence the migration patterns of trophic levels species. Pacific hake (*Merluccius productus*) that spawn off the coast of

southern California and migrate north during the spring and summer are an example of this phenomenon. Juveniles and adults feed in coastal zones of the CCS that typically correlate with areas of high phytoplankton concentrations [*Agostini et al.*, 2008]. Many other migratory species, such as Pacific Sardine (*Sardinops sagax*), albacore (*Thunnus alalunga*), and whales, also use this region to feed and spawn [*Checkley and Barth*, 2009].

Within the past several decades, the improvement of satellite-derived measurements has enabled scientists to explore seasonal and topographical influences on chl-a (as a proxy for phytoplankton) distributions in the surface ocean. The Coastal Zone Color Scanner (CZCS) was one of the first satellite missions used to map and quantify seasonal chl-a concentrations. In conjunction with CZCS-derived measurements, *Thomas et al.* [1994] and *Strub et al.* [1990] used Empirical Orthogonal Function (EOF) analysis to distinguish coastal (0 – 100km) and offshore (100 – 400km) seasonal signals. The first EOF, within the coastal region, exhibited minimum chl-a concentrations occurring during the winter months and a maximum during early summer. Conversely the first EOF was out of phase, with the offshore region displaying a minimum in chl-a during the summer months and maximum during the winter months. The coarse spatial resolution (~20km) of the CZCS limited earlier studies to large spatial (~100km) and temporal (monthly) averages to diminish the gaps and to support scientific conclusions; however, the increased resolution of new satellite missions (i.e. SeaWiFS, MODIS) provides high resolution to examine mesoscale phenomena [*Kahru and Mitchell*, 2001]. However, the patchiness (due to cloudiness) and low accuracy near shore (due to land interference and turbidity) still continue to pose challenges in efforts to explore synoptic-

scale variability within this region. Due to the difficulty with obtaining reliable, consistent measurements, numerical models offer the opportunity to investigate the importance of these rather poorly understood mesoscale processes. The GFDL CM2.6 is one such model, which offers applicable data.

1.2.2 The Physical and Biological Overview: Mesoscale Influence

Although synoptic-scale atmospheric and oceanic processes have a strong influence in this region, there are numerous mesoscale processes (i.e. jets and eddies) and features (i.e. local topography) that also influence the distribution of winds, nutrients, and biological production [*Legaard and Thomas*, 2006]. The rough topography of the CCS has been shown to impact the magnitude of upwelling events [*Huyer*, 1983]. Additionally, the surface winds can interact with the capes and headlands that exist within the CCS to intensify upwelling on a local scale [*Checkley and Barth*, 2009]. Areas on the lee of these topographical features are an especially favorable zone for phytoplankton retention growth [*Graham and Largier*, 1997]. Prior research has analyzed sections of the CCS independently, with domains selected by the seasonal differences in physical (i.e. wind stress, Ekman transport) and biological (i.e. nutrient concentrations, productivity) parameters [*Kahru and Mitchell*, 2001; *Strub et al.*, 1990; *Thomas et al.*, 1994]. In the present analysis of the CCS, this region will be divided into three subsections based on latitudinal differences in these parameters (Figure 1.3): *a. The Northern California Current System (NCCS)*, *b. The Central California Current System (CCCS)*, and *c. The Southern California Current System (SCCS)*.

a. The Northern California Current System

The NCCS is defined as the area between 41.5°N – 46.5°N, which extends from the midpoint between Cape Blanco and Cape Mendocino, moving poleward to just north of the Oregon-Washington border. With the strengthening of the NPH, the NCCS experiences peak chl-a concentrations during April-May with concentrations reaching between 3.0 mg m^{-3} to 6.0 mg m^{-3} [*Strub et al.*, 1990]. The California Current also supplies subarctic waters from the north, which are cold and nutrient-rich [*Strub and James*, 2003; *Freeland et al.*, 2003]. The winter months are characterized by downwelling-favorable winds as the AL strengthens and the NPH retreats to the south. Thus, the overall biological production diminishes during the end of fall through February. During this time period, the NCCS and the northern portion of the CCCS experience strong fluctuations in the wind strength and direction due to the passage of numerous low-pressure systems [*Dorman and Winant*, 1995]. Also, surface waters in this region typically contain high amounts of nitrate and nutrients during the winter months, but exhibit low chl-a concentrations due to light limitations [*Strub et al.*, 1987].

The coastline is relatively linear along the coast of Oregon until reaching Cape Blanco [*Dorman et al.*, 2013]. Headlands, like Cape Blanco, cause alongshore winds to be disrupted (forced over or around the orography) and biological production to be amplified [*Strub et al.*, 1990]. In addition to the subarctic input from the California Current, a significant flux of freshwater is supplied by the Columbia River, which has a variable impact based on the prevalent wind direction [*Thomas and Weatherbee*, 2006]. During upwelling-favorable wind events, the Columbia River plume can be advected downwind and offshore hundreds of kilometers [*Checkley and Barth*, 2009]. Conversely,

downwelling-favorable wind events cause the plume to remain trapped within 30km of the coastline and can be advected latitudinally at rates of about 35 km per day. This plume can act as a retention pool for phytoplankton, but the primary nutrients provided are silica and iron with little nitrate input [*Hickey et al.*, 2005].

b. The Central California Current System

The CCCS stems from about 35.5°N – 41.5°N and has fairly persistent equatorward winds throughout the spring and summer months. During the late fall and winter months, the strength of the equatorward winds diminish and are influenced by increased frequency of low-pressure systems, which generate sporadic poleward winds [*Strub et al.*, 1987a]. The wind-driven chl-a concentrations peak within 5 – 50km of the shoreline and reach concentrations above 2.0 mg m^{-3} at times [*Abbott and Zion*, 1987]. Within the CCCS, there are several headlands such as Cape Mendocino, Point Arena, and Point Sur. These capes and points disrupt the alongshore winds within the CCS. Due to these orographical features, atmospheric jets, and oceanic meanders stimulate SST and chl-a variability on timescales of three to six weeks [*Strub et al.*, 1987a]. Significant bursts in wind stress have been shown to develop south of Point Arena due to the aforementioned influence of these orographic features [*Dorman and Winant*, 1995, *Dorman et al.*, 2013] with observations displaying an average increase in wind stress south of Cape Mendocino relative to areas further north [*Dorman et al.*, 2013]. *Boe et al*. [2011] documented correlations between positive wind stress anomalies and decreased SST on the lee-side of capes and points within the CCCS and the SCCS, which indicates cold, nutrient-rich water being brought to the surface through upwelling.

c. The Southern California Current System

Unlike the NCCS and the CCCS, dynamics within the SCCS (30.5°N – 35.5°N) region more independent of the seasonal fluctuations in wind stress. Persistent, weak upwelling-favorable winds are present throughout the entire year, peaking in strength during the late summer months [*Dorman and Winant*, 1995; *Strub et al.*, 1987]. Typically, a gradient in chl-a concentrations will persist from the coastline (about 2.0 mg m^{-3}) into the offshore waters (< 0.25 mg m^{-3}) [*Strub et al.*, 1987]. Additionally the southern portion of this region, extending into Baja California, is influenced by seasonal atmospheric dynamics and by oceanic Kelvin waves associated with El Niño and La Niña [*Legaard and Thomas*, 2006]. Past research has indicated that Point Conception (~34°N) can generate upwelling-favorable winds in the lee, which is important for nutrient availability and ultimately, biological productivity in the surface ocean [*Dorman and Winant*, 1995].

1.3 DATA, MODEL ASSESSMENT, AND METHODS

1.3.1 Data

The Geophysical Fluid Dynamics Laboratory (GFDL) recently developed the Climate Model version 2.6 (CM2.6). This model has the same atmospheric and oceanic physics used in the earlier, well-documented configuration, Climate Model version 2.5 (CM2.5). The primary difference is the increased oceanic resolution of CM2.6, which has horizontal grid spacing of 4km at high latitudes and around 11km near the equator. Both CM2.5 and CM2.6 have a horizontal atmospheric resolution of 50km. The key atmospheric advancements within CM2.5 and CM2.6 over previous versions of the GFDL suite of climate models (CM2.0 – CM2.4) lies within the physics, the increased

amount of vertical levels (i.e. upper troposphere and stratosphere), and enhanced cloud parameterization schemes [*Delworth et al.*, 2012]. Otherwise, the atmospheric physics are the same as found in the GFDL global atmosphere and land model simulations [*GFDL Global Atmospheric Model Development Team*, 2004]. In addition to the finer resolution, the oceanic physics have been enhanced to simulate more energetic and realistic ocean dynamics. The main additions include the increased submesoscale eddy activity, lower viscosity, and K-profile parameterized vertical mixing, which provide a better representation of the real environment. The exchange between the atmosphere and the ocean is designed to occur once an hour.

The dynamically coupled ecosystem model of CM2.5 and CM2.6 is known as Carbon Ocean Biogeochemisty and Lower Trophics (COBALT). Relationships among physical properties in CM2.6 and plankton dynamics are examined using COBALT. COBALT uses 13 nitrogen-based state variables to best represent the global planktonic food web. The three primary phytoplankton groups (small phytoplankton, large phytoplankton, and diazotrophs) all uptake nitrogen and ammonia. The key productivity limitations that influence the productivity of these organisms are light availability and nutrient concentrations (i.e. nitrate, phosphorus, and iron) as previously indicated by *Spitz et al.* (2003). Vertical sinking, zooplankton grazing, and viral shunting are all included and contribute to phytoplankton loses. Remineralization is also integrated to reintroduce ammonia to the system. A more in-depth explanation of the nutrient dynamics (including phosphorus and iron grazing) and other formulations used in COBALT can be found in *Stock et al.* [2014].

A two-year time series of daily CM2.6 model data and a twenty-year time series of monthly CM2.6 model data was acquired through collaboration between the University of South Carolina and GFDL. These model runs do not incorporate any future climate scenarios, but instead assume greenhouse-gas composition similar to 1990. In this study, the primary environmental parameters utilized from the daily CM2.6 model runs were surface chl-a concentrations ($\mu g\ L^{-3}$), wind stress ($N\ m^{-2}$), SST (°C), nitrate concentration ($\mu g\ m^{-3}$), pH, and primary production in the upper 100m ($mol\ m^{-2}\ s^{-1}$). This study used daily averages of the CM2.6 data at a 1/10° resolution. The monthly averaged CM2.6 data (20-year time series) was regridded to a lower resolution (1/2°) to compare against the satellite-derived chl-a and wind stress measurements (further described in Section 1.3.2). Data processing, manipulation, and analysis were completed using MATLAB2012b.

1.3.2 Model Assessment

The goal of the model assessment is to explore the CM2.6 model's representation of the surface wind patterns and chl-a concentrations within the CCS in comparison to satellite-derived data. The limited availability and lack of previous utilization of CM2.6 motivates this assessment. *Kahru and Mitchell* [2001] produced a blended surface chl-a satellite product focused on the CCS that incorporates estimates of chl-a from numerous satellites (i.e. SeaWiFS, MODIS, MERIS) in an attempt to improve spatial and temporal resolution within the region. The blended chl-a product has been compared against ship-based observations [*Kahru and Mitchell*, 1999], which were deemed to be accurate and representative of the chl-a concentrations within the CCS. Similar to the satellite-derived chl-a data, wind stress data used for this validation are from a blended satellite product

entitled Blended SeaWinds. This product combines previous and recent satellite missions (i.e. QuikSCAT, TMI, and AMSR-E) to lengthen the time series of wind estimates while improving the spatial and temporal resolution [*Zhang et al.*, 2006]. The Blended SeaWinds product has been previously compared against observational NDBC buoy measurements and has demonstrated a significant correlation both offshore and inshore [*Garcia-Reyes and Largier*, 2010]. Given the robustness of the chl-a and wind stress datasets, both are adopted as observationally based products for comparison with CM2.6 within the CCS. A 20-year time series of monthly averages was compiled for CM2.6, and monthly averages were calculated from the daily satellite-derived products for a 14-year period to create climatological means for comparison.

As previously mentioned in Section 1.3.1, both model and satellite-derived datasets were linearly interpolated to 1/2° grid spacing to complete a direct comparison. Figure 1.4 (Figure 1.5) represents the average of spatial distribution of chl-a during the summer (winter) for both model and satellite-derived datasets. The satellite-derived measurements indicate large concentrations of chl-a nearshore during the summer and a steep gradient between the coastal zones extending offshore into open ocean waters during the winter months. Although CM2.6 expresses the general spatial distribution of chl-a nearshore and offshore, the model underestimates the magnitude nearshore and overestimates the offshore chl-a concentrations with respect to the satellite-derived measurements. CM2.6 is able to replicate the spatial patterns as well as the peak nearshore chl-a concentrations fairly well. However, CM2.6 underestimates the chl-a concentrations patterns nearshore and overestimates the offshore concentrations, which has been previously documented [*Stock et al.* (2014)].

The CM2.6 model data were assessed against satellite-derived measurements by comparing the average daily values. Both chl-a and meridional wind stress (τ_y) time series were generated from averages between 0 – 100km (nearshore) and 100 – 300km (offshore) within the NCCS, CCCS, and SCCS. Differences between the nearshore and offshore time series exist within all three regions of the CCS. Within the NCCS (Figure 1.6), CM2.6 does not represent the amplified nearshore spring-summer chl-a concentrations (Figure 1.6a). Both offshore time series within the NCCS indicate a spring-summer chl-a minimum, which has been revealed by past research [*Strub et al.*, 1990]. Within the CCCS, CM2.6 does not capture the nearshore (Figure 1.7a) spring and fall chl-a maxima that are represented by the satellite-derived measurements. The summer chl-a minima are characterized in the offshore (Figure 1.7b) CM2.6 time series, but CM2.6 overestimates the winter chl-a concentrations. Within the SCCS, the nearshore (Figure 1.8a) CM2.6 chl-a concentrations are better represented, but overestimate the offshore chl-a concentrations throughout most seasons (Figure 1.10b). CM2.6 τ_y estimates, within the NCCS, display a strong seasonal similarity to the satellite-derived time series in the nearshore (Figure 1.6c) and offshore (Figure 1.6d) time series. However, CM2.6 overestimates the magnitude of the offshore τ_y during the fall and winter months when compared to the satellite-derived product. Similarly to the NCCS, the daily τ_y events express comparable seasonal trends in the nearshore and offshore within both the CCCS (Figure 1.7c and 1.7d) and SCCS (Figure 1.8c and 1.8d). Although these two parameters (chl-a and τ_y) express differences in concentration and magnitude between CM2.6 and satellite-derived measurements, CM2.6 captures the

spatial distribution well within in the CCS, warranting its use for the remainder of this study.

1.3.3 Methods

a. Extracting the High- and Low-Frequency Events

First, the Global Self-consistent, Hierarchical, High-resolution Shorelines [*Wessel and Smith,* 1996] was used to estimate a distance grid from the coastline region between 30.5°N – 46.5°N and 133.0°W – 114.0°W at the 1/10° resolution, for each grid cell. Thresholds were set at different intervals to characterize three distance ranges offshore. The first distance range offshore is from 0 – 25km (Band 1). Band 1 is characterized as a narrow band of coastal upwelling within 25km of the coastline [*Huyer*, 1983]. The second distance range is between 25 – 100km (Band 2). Band 2 experiences filaments and coastal plumes that extend off the coastline [*Abbott and Zion*, 1987]. The third distance range is between 100 – 300km (Band 3). Band 3 is characterized as an area that has drastic decreases in phytoplankton concentrations in relation to the nearshore environment [*Thomas et al.*, 1994; *Strub et al.*, 1990]. These three offshore ranges are shown in Figure 1.3. This grid was then applied to the CM2.6 model data to extract the data for all parameters (chl-a, τ_y, nitrate, etc.) within each of the ranges. Finally, the model data was divided into three latitudinal regions, NCCS (~41.5°N – 46.5°N), CCCS (~35.5°N – 41.5°N), and SCCS (~30.5°N – 35.5°N), as previously described in sections 1.2.2a, 1.2.2b, and 1.2.2c, respectively. Daily spatial averages within each of the bands and regions were then calculated, resulting in a two-year time series of daily averages for each parameter.

After acquiring each time series, a simple averaging scheme was applied to extract the high-frequency (3 – 7 days) and low-frequency (7 – 30 days) signals from each parameter. First, each time series was detrended to remove any negative or positive trend found within the CM2.6 model data. Applying a 30-day running average to the detrended, 2-year time series dampened the seasonal signal. The 30-day average was then subtracted from the original time series to acquire the anomalous events less than 30 days (30-day bandpass filter), as shown in Figure 1.9. To obtain the high-frequency events, the events less than 3-days and greater than 7-days must be removed from the 30-day bandpass. A 3-day running mean was then applied to the 30-day bandpass to acquire all events greater than 3-days. Also, a 7-day running mean was applied to the 30-day bandpass to acquire all events greater than 7 days. The 3-day running mean was subtracted from the bandpass-filtered time series to acquire events less than 3 days (3-day bandpass) and the 7-day running mean was subtracted from the 30-day bandpass to acquire events less than 7 days (7-day bandpass). The high-frequency events were then extracted by subtracting the 3-day bandpass from the 7-day bandpass, as shown in Figure 1.10. Finally, the low frequency events were acquired by subtracting the 7-day bandpass from the 30-day bandpass, as shown in Figure 1.11. This averaging scheme was applied to all parameters and spatial subsections.

b. Statistical Methods

Using the high- and low-frequency time series for each parameter, the cross-correlation function (via MATLAB) was applied to estimate the lag and conduct a correlation between each paired time series (i.e. chl-a vs. τ_y) to acquire the maximum correlation coefficient (r), and p-value (p). The lag at which r was maximized was taken

as an indication of the primary response period between chl-a and τ_y at both high-frequency (Figure 1.10) and low-frequency (Figure 1.11) events. To estimate the response time of other parameters (chl-a, SST, nitrate, etc.) to τ_y, the focus was only on the positive lag since the parameters should be a response to the wind event (i.e. high chl-a concentrations should be generated by a wind event, not vice versa). Also, a 30-day threshold was applied to limit the lag values to less than 30-days given that any correlations outside of that time period are likely spurious. For example, Figure 1.12 displays the correlation between chl-a and τ_y within Band 1 of the CCCS at various lags, from 0 days to 30 days. Figure 1.12a illustrates that the peak correlation occurs with a lag of 0 days ($r = 0.236$; $p << 0.0001$). Figure 1.12b displays the low-frequency lag as 4 days ($r = -0.517$; $p << 0.0001$). In addition to conducting this analysis on the full 2-year time series (Section 1.4.1), the time series were broken down into seasonal time series (Section 1.4.2); thus, the summer months and winter months were extracted to form a summer and winter time series at each location and for both parameters.

1.4 RESULTS

As expressed in Section 1.3.3b, the frequency analyses compared time series of chl-a with τ_y, and the temporal lags that exhibited the greatest correlations between the two time series were identified. Each time lag was examined with respect to all three regions and each of the three offshore bands. A correlation was applied to the lagged time series to acquire the correlation coefficients (r). Negative r-values indicate a positive response between chl-a concentrations to upwelling-favorable τ_y events at the high- and/or low-frequency. Figure 1.13 is an example within Band 1 of the CCCS; the highest correlation was evident at a lag time of 4 days between low-frequency chl-a

concentrations and τ_y events. Figure 1.14 indicates that a significant correlation exists between chl-a concentrations and τ_y within Band 1 of the CCCS at low-frequency ($r = -0.517$; $p << 0.0001$). The frequency analysis was applied to the various chl-a and τ_y time series within the CCS with respect to the three regions and three offshore bands, which yielded an array of optimal lags, correlation coefficients (r), and levels of significance (p-value).

1.4.1 Two-year time series

The chl-a and τ_y time series at high-frequency exhibit weak relationships within the CCS. Although statistically significant, the NCCS and CCCS both demonstrate small correlation coefficients as shown in Figure 1.15. Within the SCCS, chl-a and τ_y do not show any significant relationship between one another in any of the three offshore bands. On average, greatest correlations in all regions and bands were found at a lag between 0 – 2 days.

The low-frequency time series showed similar trends between the three regions within the CCS as well as the three offshore bands (Figure 1.15). The NCCS, CCCS, and SCCS all express similar offshore trends with the highest negative correlations occurring in Band 1. Figure 1.15 shows the significant correlations in Band 1 for the NCCS ($r = -0.581$; $p << 0.0001$), CCCS ($r = -0.517$; $p << 0.0001$), and SCCS ($r = -0.359$; $p << 0.0001$). The correlation coefficients become more positive in Band 2 as the chl-a and τ_y time series exhibit less correlation than those time series near the coast. A significant correlation was noted within the NCCS ($r = -0.433$; $p << 0.0001$) and CCCS ($r = -0.415$; $p << 0.0001$), however, there was a much weaker relationship within the SCCS ($r = -0.163$; $p << 0.0001$). In Band 1 and Band 2, the chl-a time series lagged the τ_y time series

by 4 – 6 days in all three regions. In Band 3, the relationship between chl-a concentrations and τ_y diminishes in all three regions: NCCS (r = -0.156), CCCS (r = -0.171), and SCCS (r = -0.180) at an optimal lag of 30 days.

1.4.2 Summer time series

During the summer months, the high-frequency time series within the NCCS and CCCS display statistically significant, negative responses between chl-a concentrations and τ_y within Band 1 (r = 0.518; r = 0.436, respectively) at a 0-day lag. Figure 1.16a indicates that the second and third offshore bands within the NCCS have no significant relationships between the chl-a concentrations and τ_y. However, the CCCS shows a positive response in chl-a concentrations in Band 2 ($r = -0.346$; $p << 0.0001$) and Band 3 ($r = -0.370$; $p << 0.0001$) at a 2-day lag. The high-frequency time series in the SCCS exhibits no significant relationships in any of the three offshore bands during summer.

At low-frequency τ_y events, the chl-a responds positively at a 4- to 5-day lag in Band 1 ($r = -0.495$; $p << 0.0001$) and Band 2 ($r = -0.638$; $p << 0.0001$) within the NCCS. Figure 1.16a shows a negative response within the CCCS in Band 1 ($r = 0.224$; $p < 0.01$) and a positive response in Band 2 ($r = -0.301$; $p << 0.0001$) and Band 3 ($r = -0.314$; $p << 0.0001$). The SCCS displays a 4- to 5-day lag between chl-a concentrations and low-frequency τ_y events within Band 1 ($r = -0.377$; $p << 0.0001$) and Band 2 ($r = -0.203$; $p < 0.01$).

1.4.3 Winter time series

During the winter months, the high-frequency time series within the NCCS display a weak, negative response within Band 1 ($r = 0.281$; $p << 0.0001$) and Band 2 (r =

2.89; $p << 0.0001$) at a 0-day lag. No statistical significance exists at any of the three offshore bands within the CCCS and SCCS.

A significant positive response is exhibited in Band 1 within the NCCS ($r = -0.645$; $p << 0.0001$) and CCCS ($r = -0.402$; $p << 0.0001$) at a 4- to 5-day lag. This significant relationship weakens further offshore (Figure 1.16b). None of the three bands express statistical significance within the SCCS.

1.5 DISCUSSION AND CONCLUSIONS

The primary purpose and focus of this study was to investigate the response of surface chl-a to high- and low-frequency τ_y events. High-frequency τ_y events were hypothesized to have a weak correlation with chl-a concentrations, as wind events at this frequency (3 – 7 days) may not persist long enough to stimulate a significant shoaling of the nutricline to produce a significant response in surface chl-a concentrations. Rather, the τ_y events at low-frequency (7–30 days) were hypothesized to raise the nutricline for a period long enough to sustain a chl-a response. This relationship was hypothesized to be more significant during the summer months than the winter months due to the primary limitation to summer primary productivity being availability of nutrients, which upwelling can decrease the impact of that limitation by supplying nutrients to the euphotic zone. The frequency analysis highlighted relationships in both the two-year time series and the seasonal (summer and winter) time series that will be addressed in the succeeding subsections: 1.5.1 Two-year time series and 1.5.2 Seasonal time series.

1.5.1 Two-year time series

In general, the three regions within the CCS all display weak relationships between chl-a concentrations and high-frequency τ_y events. Past research studies have

indicated that high-frequency upwelling events occur within the CCS [*Huyer*, 1983], the Benguela Current System [*Desbiolles et al.*, 2014], and other EBUS. Anomalously low coastal SSTs (satellite-derived) and increased water densities (observational) were used to quantify the cold, dense waters forced to the surface during these upwelling events. *McGowan et al*. [2003] expressed that the thermocline and nutricline reside at similar depths within the water column, which would indicate that high-frequency wind events generating cold SST anomalies near the coastline would also be introducing new nutrients into the euphotic zone. However, the weak correlation between high-frequency τ_y events and chl-a concentrations found in the CCS regional results implies that upwelled nutrients may not persist long enough in the euphotic zone to sustain a significant phytoplankton bloom or the model may be misrepresenting these events.

Past research has used model estimations to propose that wind speed and direction must be relatively static for a minimum duration of 3 – 4 days to have an ecological significance, which was approximated as the amount of time necessary for phytoplankton to complete nutrient uptake [*Botsford et al.*, 2006]. Although, τ_y events at frequencies between 2 – 6 days, typically driven by atmospheric frontal passages or weather-bands, can interrupt upwelling long enough to decrease primary productivity [*Bane et al.*, 2007]. Also, *Michaelsen et al.* [1988] proposed that phytoplankton response time is not fast enough to react to every high-frequency meteorological event (cycle between 5 – 6 days) and may not sustain a phytoplankton bloom, but rather prime the surface ocean for future blooms in primary productivity.

At low-frequencies, all three regions within the CCS displayed significant, positive responses between τ_y events and chl-a concentrations in Band 1 (Figure 1.15).

Bane et al. (2007) found similar results in modeled phytoplankton responses off the coast of Oregon (~43.5°N – 45.5°N), which were at a 7-day lag to low-frequency τ_y events. The cause of these τ_y events in this area were attributed to fluctuations in the position of the jet stream, which were persistent long enough to bring sufficient amounts of nutrients to the euphotic zone and stimulate primary productivity [*Bane et al.*, 2007]. Weaker offshore relationships between τ_y and chl-a concentrations within the CCS may be attributed to a few different factors such as eddy activity, submesoscale jets and squirts, and deepening mixed-layer depth. In the NCCS and CCCS, Band 3 displayed weak relationships between chl-a and τ_y, which may be attributed to deeper mixed layers in these regions [*Marchesiello et al.*, 2003; *Strub et al.*, 1991]. The weak correlations in Band 2 and Band 3 of the SCCS may be due to weaker τ_y events or deeper stratification, which would both minimize the amount of nutrients reaching the surface [*Huyer*, 1983]. Additionally, eddy and other mesoscale activity increases offshore (i.e. Band 2 and Band 3), which can cause decreases in this proposed linear relationship between chl-a concentrations and τ_y events [*Strub et al.*, 1991].

1.5.2 Seasonal time series (Summer vs. Winter)

a. The Northern California Current

The significant seasonal variability within the CCS's atmospheric and oceanic physical factors, such as sea-level pressure, SST, nutrient abundance, and light availability, prompted an individual assessment and comparison of the summer and winter timeframes. Weak relationships between chl-a and high-frequency τ_y events exist within the NCCS during both summer and winter months. This is potentially due to wind events interrupting upwelling and the subsequent nutrient flux, which ultimately, can

decrease primary production [*Bane et al.*, 2007]. However, the anomalously negative response in chl-a concentrations that exists within Band 1 of the NCCS (Figure 1.16a) may be attributed to the weak relationship between τ_y events and surface nitrate (Figure 1.17), which is expressed by a low correlation coefficient. These relationships between chl-a concentrations (and nitrate) and τ_y, in Band 1 of the NCCS, were calculated at a 0-day lag; therefore, a negative response between chl-a and τ_y events would indicate that wind-driven upwelling events do not simultaneously drive biological production. At low-frequencies, the strong relationships between chl-a concentrations and τ_y events exist in both summer and winter. Chl-a concentrations appear to be highly correlated to coastal τ_y events (Band 1 and Band 2) in both seasons, which is consistent with the findings of *Bane et al*. [2007]. This indicates that low-frequency τ_y events that oscillate between downwelling- and upwelling-favorable events persist long enough to impact chl-a concentrations negatively or positively, respectively.

b. The Central California Current System

High-frequency events within the offshore bands (Band 2 and Band 3) exhibit significant correlations during the summer, but not the winter. During the summer, these weak offshore correlations between chl-a concentrations and τ_y events could be linked to intensified mixing [*Legaard and Thomas*, 2006]. Also, *Henson and Thomas* [2007] conveyed that light limitations during the winter could drastically hinder phytoplankton growth, even if sufficient nutrients are present. At low frequencies, the CCCS displays significant differences between the winter and the summer. During the winter, relationships between the τ_y events and chl-a concentrations may be attributed to oscillations in the jet stream due to these events occurring on time scales of 10 – 40 days

[*Bane et al.*, 2007]. However, during the summer, negative response exists within Band 1, which appears to be anomalous and due to coastal eddy activity [*Hayward and Mantyla*, 1990].

Spatial maps were visually analyzed to determine the relative magnitude of eddy activity within 300km of the coastline. Figure 1.18 displays eddy activity in Year 1 to be more active, relative to Year 2 (Figure 1.19), within the CCCS as a whole and specifically nearshore to Cape Mendocino (~39°N). September 4 (Figure 1.18) shows the influence of several anticyclonic eddies within Band 1 and Band 2 of the CCCS, which lowers the surface chl-a concentrations. The presence of these features would cause deviations from the linear relationship between chl-a concentrations and τ_y events [*Hayward and Mantyla*, 1990]. Conversely, Figure 1.19 shows minimal nearshore eddy activity throughout the Year 2 summer, with respect to Year 1 summer (Figure 1.18).

To further investigate this nearshore anomaly within the CCCS, the summer time series was divided into Year 1 summer (Figure 1.20a) and Year 2 summer (Figure 1.20b) to determine if there were any statistical variations between the two years. A weak response in chl-a concentrations is shown in Band 1 during increased eddy activity (Year 1) and a strong, positive response between chl-a concentrations and τ_y events during decreased eddy activity (Year 2). Past research has demonstrated that persistent eddies near Cape Mendocino and other headlands can disperse nutrients and phytoplankton away from the coastline [*Strub et al.*, 1991; *Hayward and Mantyla*, 1990], which would weaken the relationship between τ_y events and chl-a concentrations.

c. The Southern California Current System

High-frequency events within the SCCS experience extremely weak relationships at all three offshore bands in both summer and winter, which coincides with the theory that decreases in primary productivity can be generated from events at this frequency [*Bane et al*., 2007]. However, at low-frequencies, the summer months display a more significant relationship within the first two bands than the winter. These statistically insignificant relationships during the winter months may be due to decreased light availability [*Henson and Thomas,* 2007] or deep mixed layer depth [*Huyer*, 1983], which would more readily mix nutrients and phytoplankton out of the euphotic zone. Ultimately, these relationships within the SCCS indicate that low frequency τ_y events may be more ecologically significant during the summer than the winter.

1.5.3 Conclusions and Importance

In general, high-frequency (3 – 7 days) τ_y events were found to have a minimal impact on chl-a concentrations throughout the CCS. However, low-frequency τ_y events were shown to have a significant relationship with chl-a concentrations within 100km of the coastline in the NCCS and CCCS, and within 25km in the SCCS. Furthermore, this positive relationship was more significant during the summer within the CCCS (Band 2 and Band 3) at high-frequencies and SCCS (Band 1) at low frequencies. Also, enhanced eddy activity has been proposed to generate discontinuities between the linear relationships of alongshore wind events and chl-a concentrations [*Strub et al.*, 1991; *Hayward and Mantyla*, 1990].

These results suggest that high-frequency upwelling events may not have any immediate significance on the chl-a concentration. However, *Michaelsen et al.* [1988]

proposed that τ_y events at this frequency could possibly prime the system for blooms at a later period, which should be further researched. *Henson and Thomas* [2007] conveyed that persistent upwelling-favorable τ_y events greater than 15 days could initiate seasonal primary productivity within the CCS; thus, the importance low-frequency events could have implications on spring productivity. Future work should attempt to include the utilization of the full, three-dimensional CM2.6 model data for a more extensive analysis of the vertical oceanic dynamics within the CCS. Additionally, future improvements in temporal and spatial resolution of satellite-derived measurements may allow for similar frequency analyses to be applied.

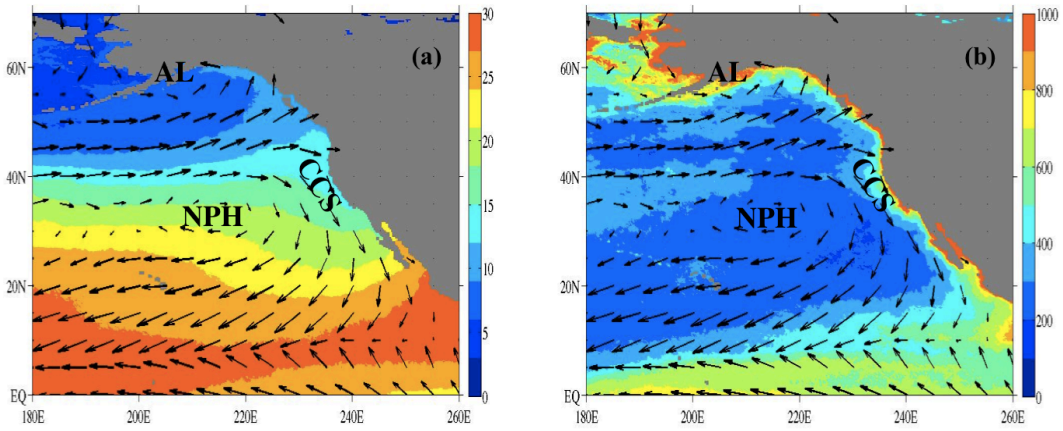

Figure 1.1: (a) Annual Advance Very-High Resolution Radiometer-derived sea surface temperature (°C) and (b) *Epply* [1972] estimated net primary production (mg Carbon m^{-2} day^{-1}). Satellite-derived QuikSCAT estimated 10-meter winds are overlaid.

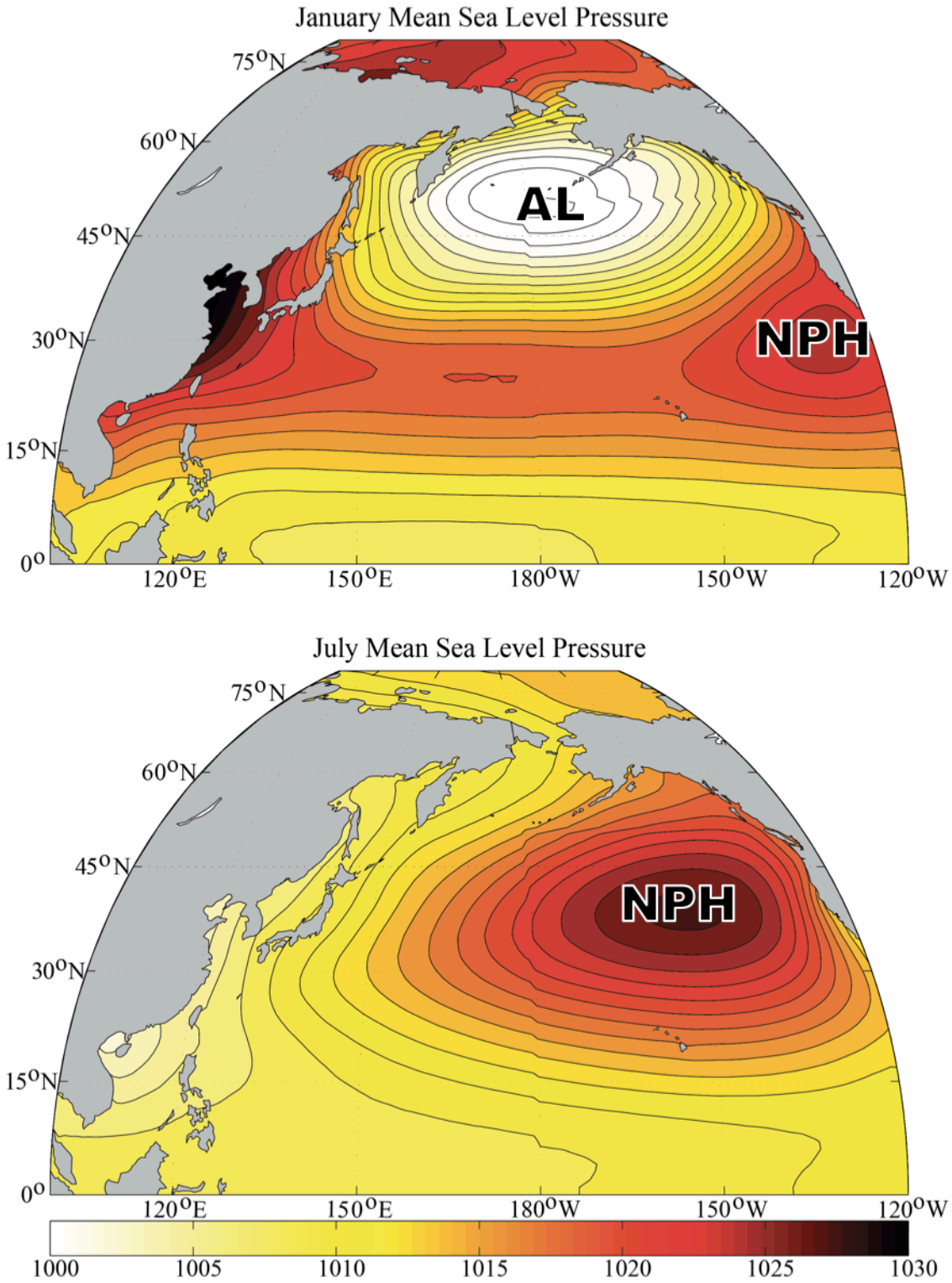

Figure 1.2: (a) Average January and (b) July sea level pressure (mb), generated from a 10-member ensemble from 1861-2100 (RCP8.5).

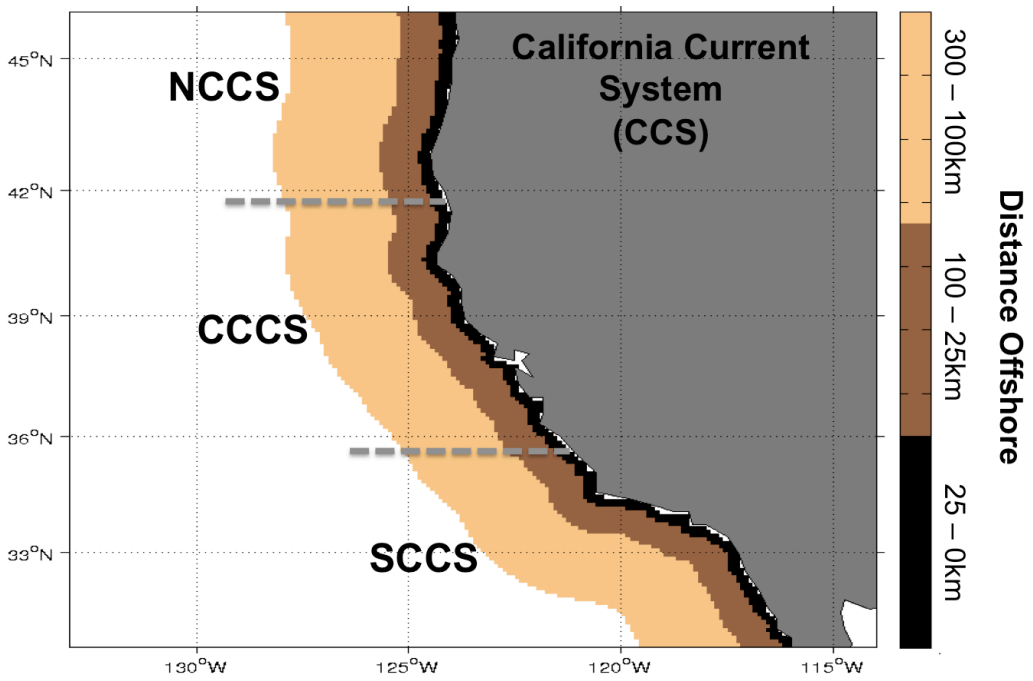

Figure 1.3: Spatial grid of the CCS, divided into three subsections: Northern CCS (NCCS), Central CCS (CCCS), and the Southern CCS (SCCS). Each subsection was divided into three offshore bands: 0 – 25km (Band 1), 25 – 100km (Band 2), and 100 – 300km (Band 3).

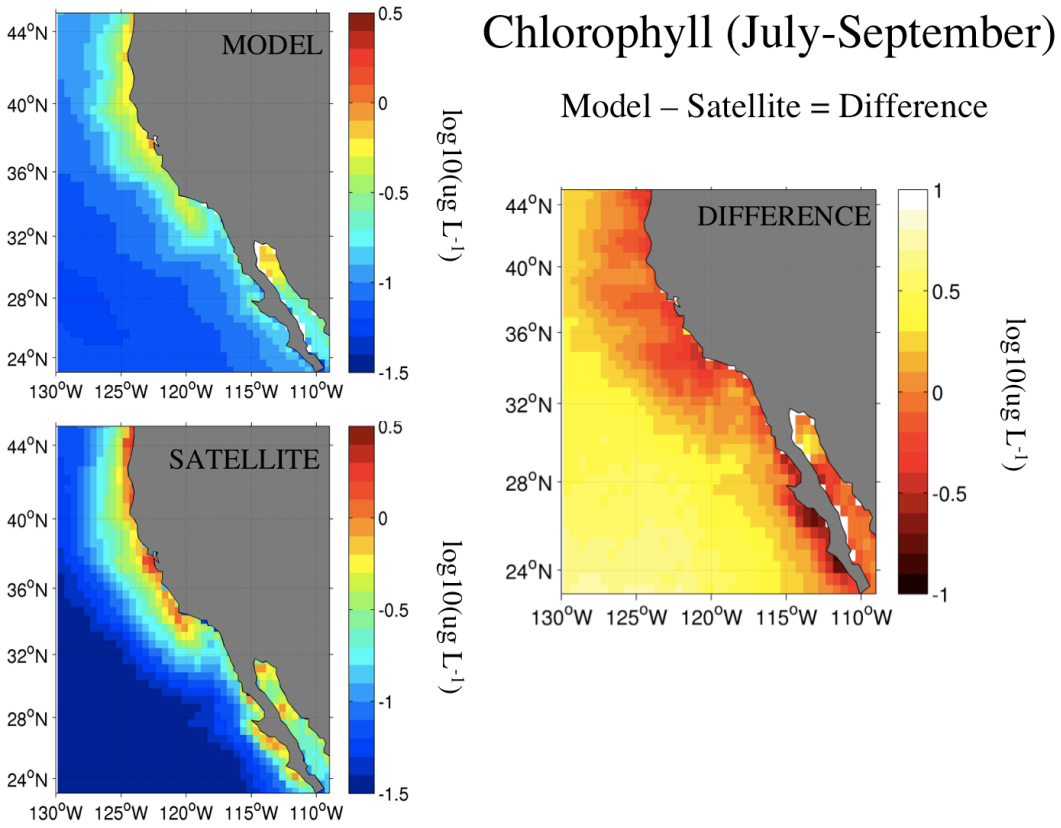

Figure 1.4: Difference between model-estimated and satellite-derived average chl-a (log(ug L^{-1})) for July-September.

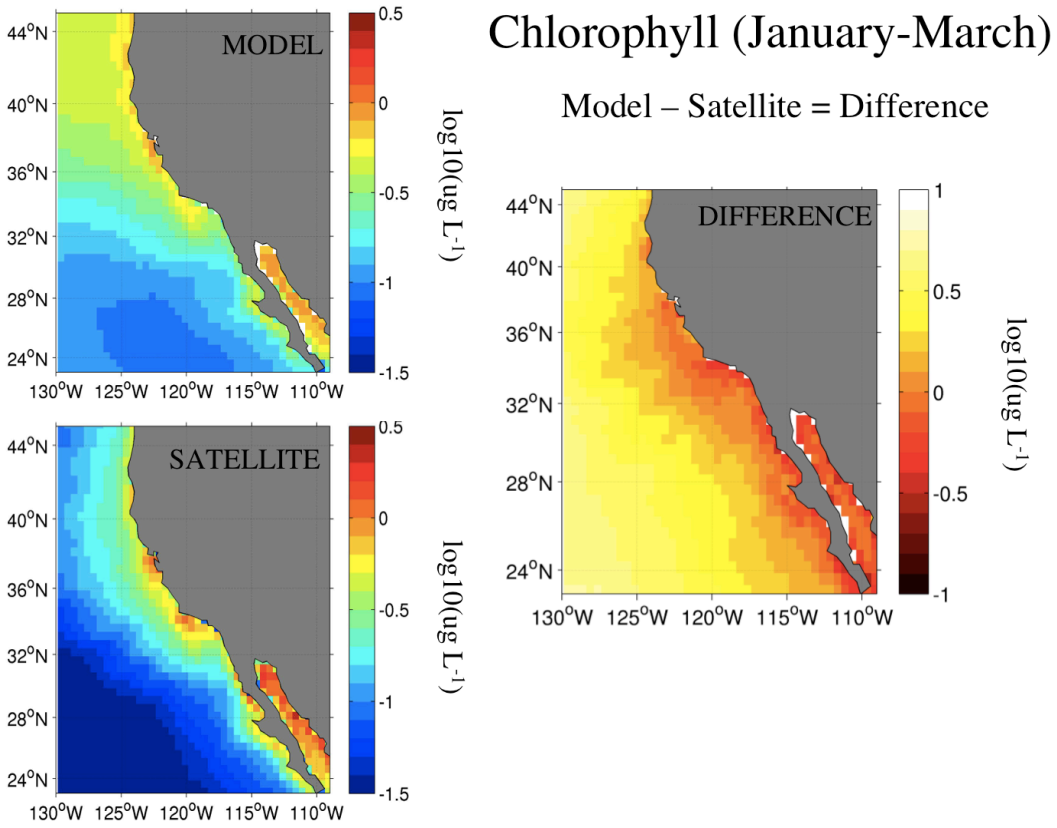

Figure 1.5: Difference between model-estimated and satellite-derived average (log(ug L^{-1})) for January-March.

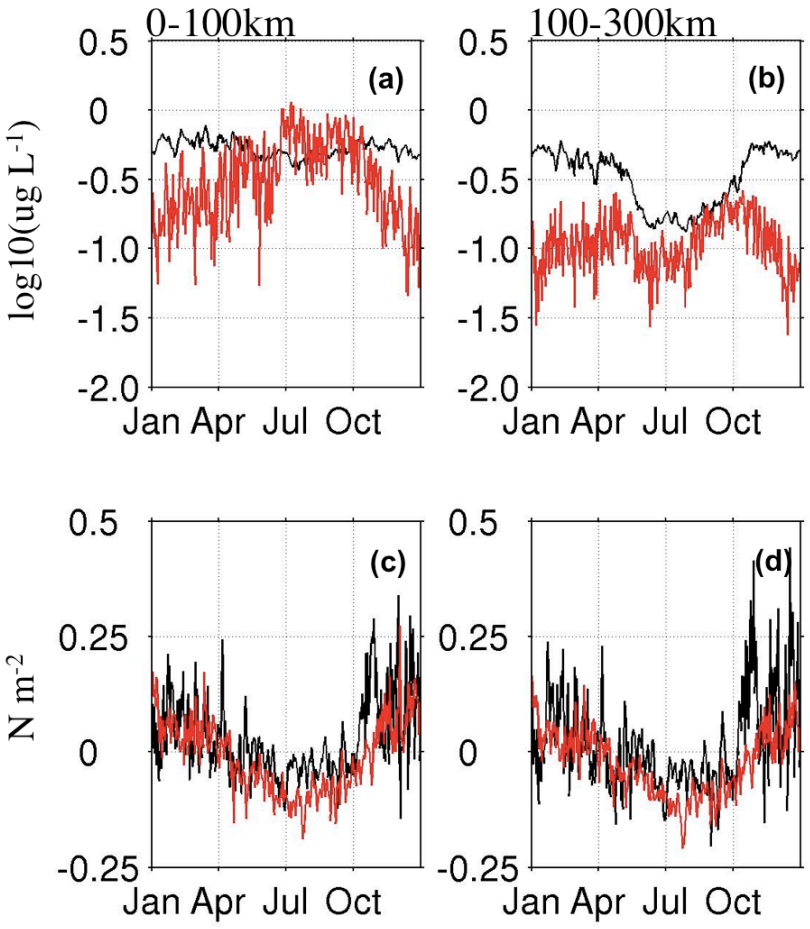

Figure 1.6: Average daily chl-a (log(ug L^{-1})) estimates in the NCCS (a) nearshore and (b) offshore. Average daily τ_y (N m^{-2}) estimates in the NCCS (c) nearshore and (d) offshore. Black lines indicate CM2.6 and the red lines indicate satellite-derived measurements.

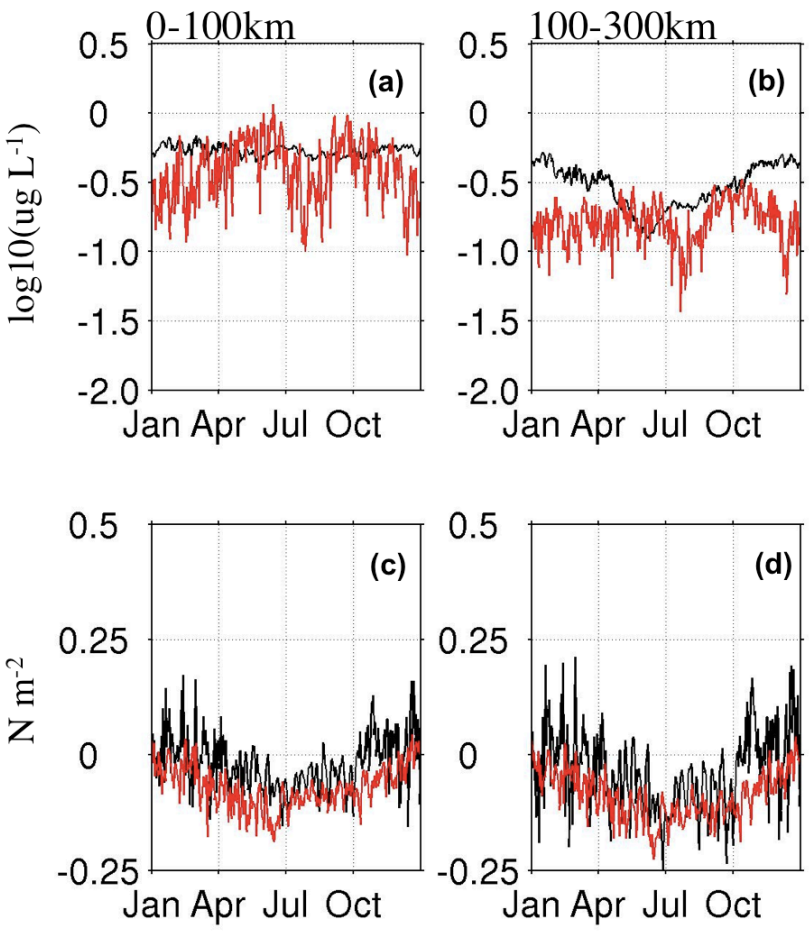

Figure 1.7: Average daily chl-a (log(ug L^{-1})) estimates in the CCCS (a) nearshore and (b) offshore. Average daily τ_y (N m^{-2}) estimates in the CCCS (c) nearshore and (d) offshore. Black lines indicate CM2.6 and the red lines indicate satellite-derived measurements.

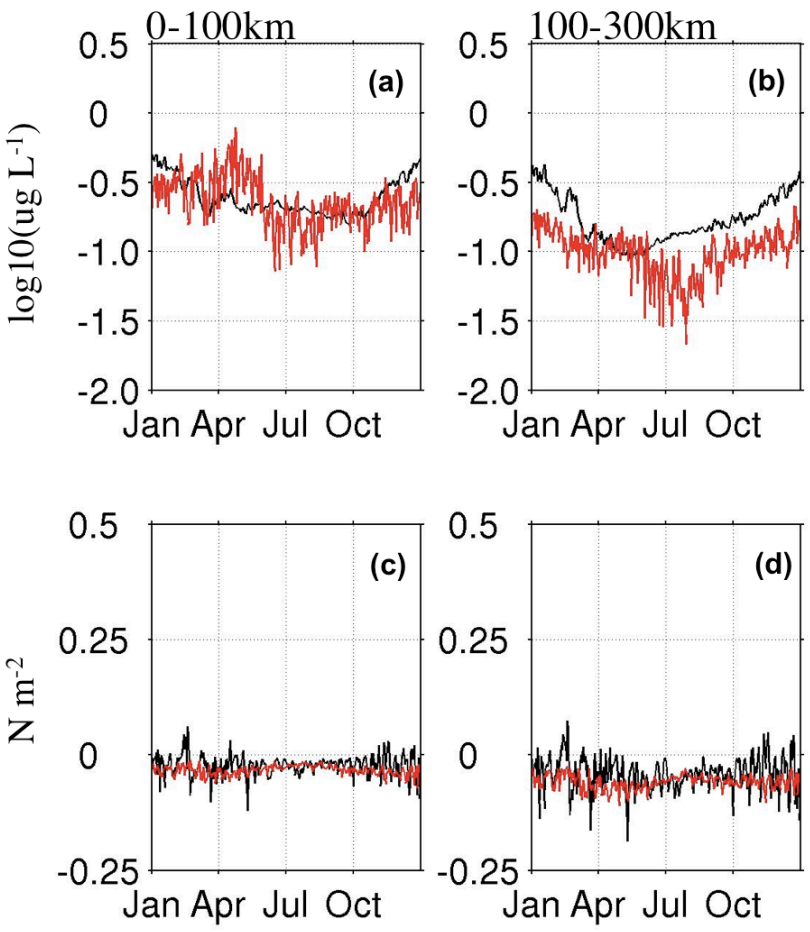

Figure 1.8: Average daily chl-a (log(ug L^{-1})) estimates in the SCCS (a) nearshore and (b) offshore. Average daily τ_y estimates in the SCCS (c) nearshore and (d) offshore. Black lines indicate CM2.6 and the red lines indicate satellite-derived measurements.

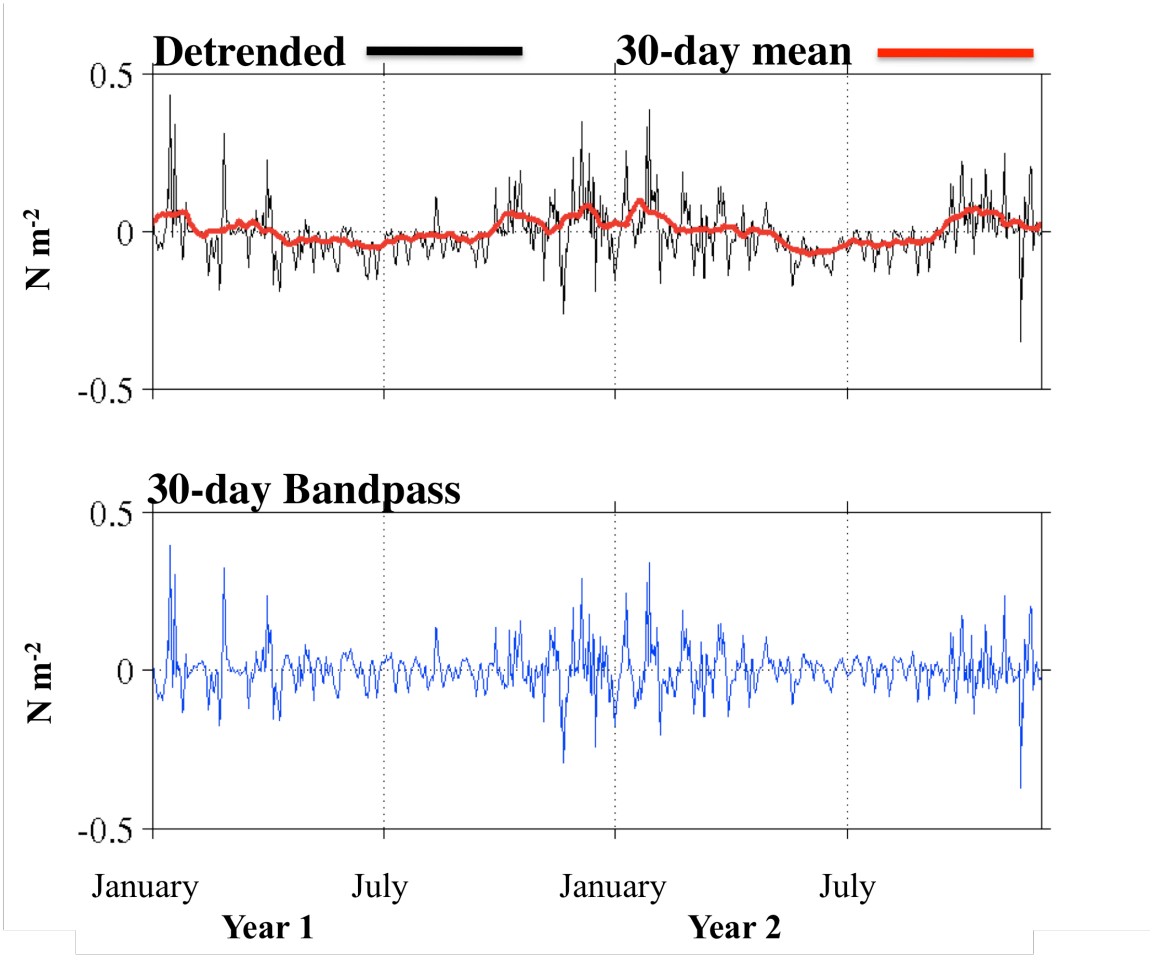

Figure 1.9: Example of the detrended time series and 30-day bandpass for τ_y (N m^{-2}).

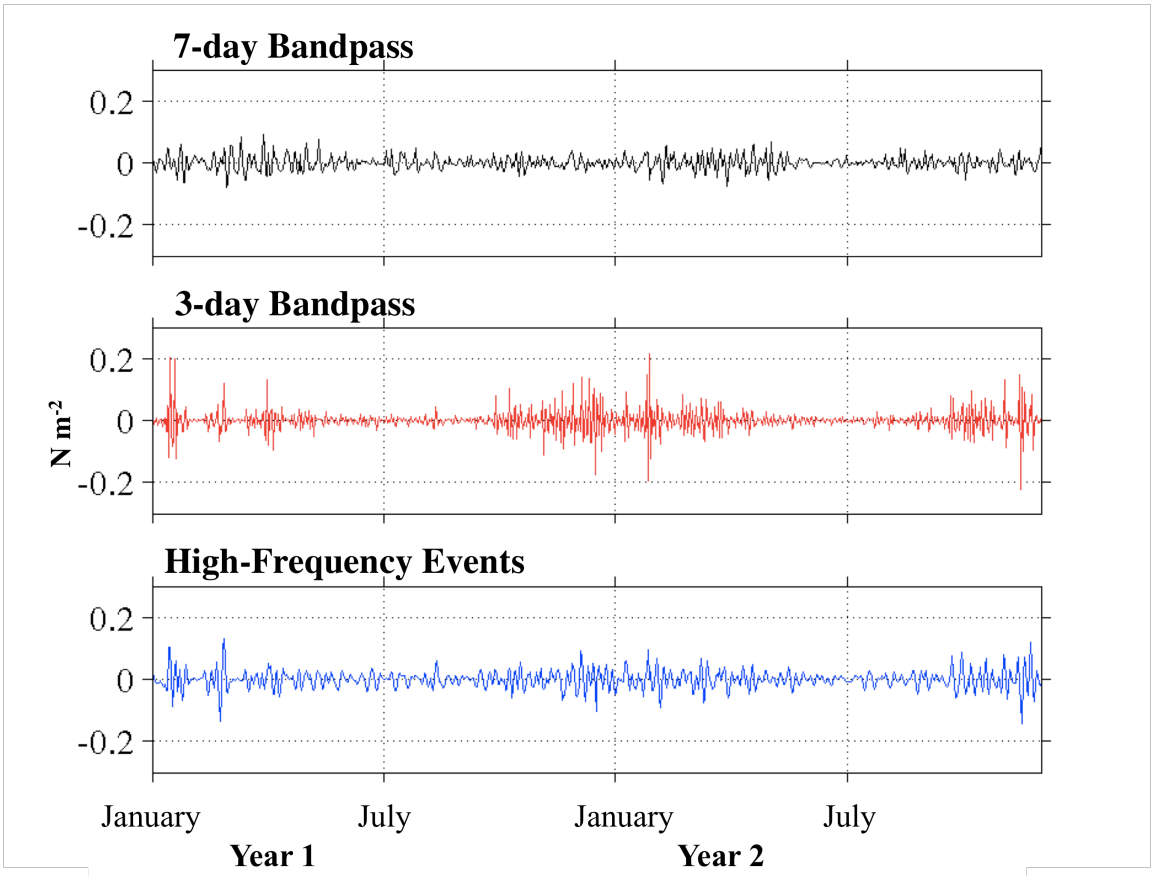

Figure 1.10: Example of the 7-day bandpass, 3-day bandpass, and high-frequency for τ_y (N m^{-2}).

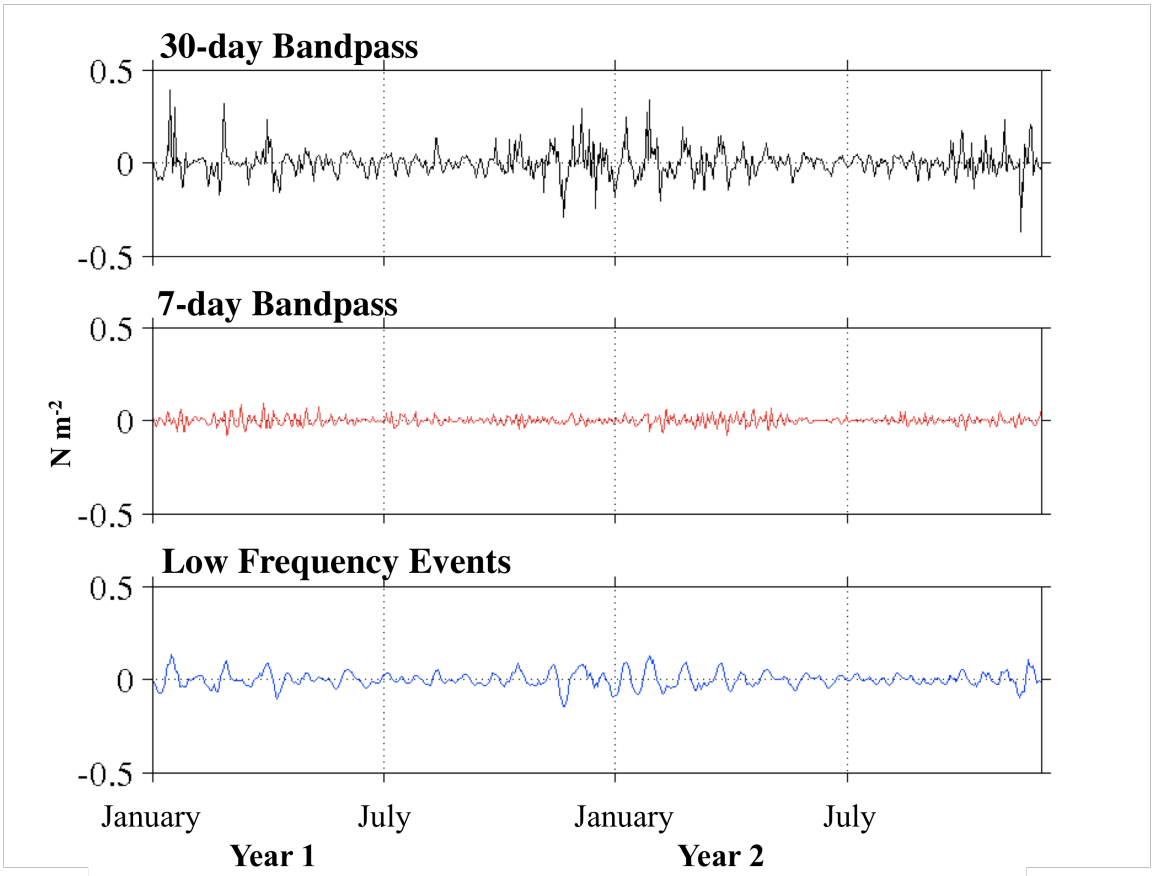

Figure 1.11: Example of the 30-day bandpass, 7-day bandpass, and low-frequency for τ_y (N m^{-2}).

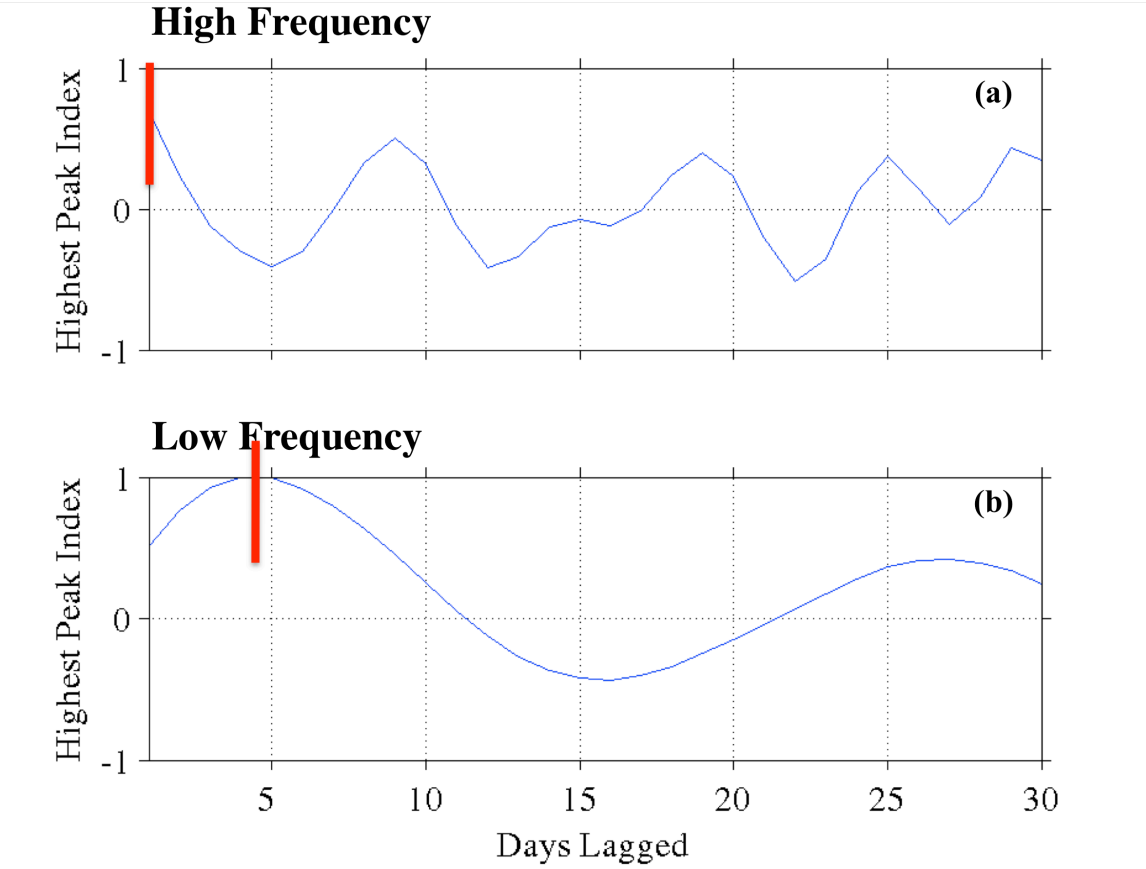

Figure 1.12: Example of the lag between chl-a (log(ug L^{-1})) and τ_y (N m^{-2}) at (a) High Frequency and (b) Low Frequency.

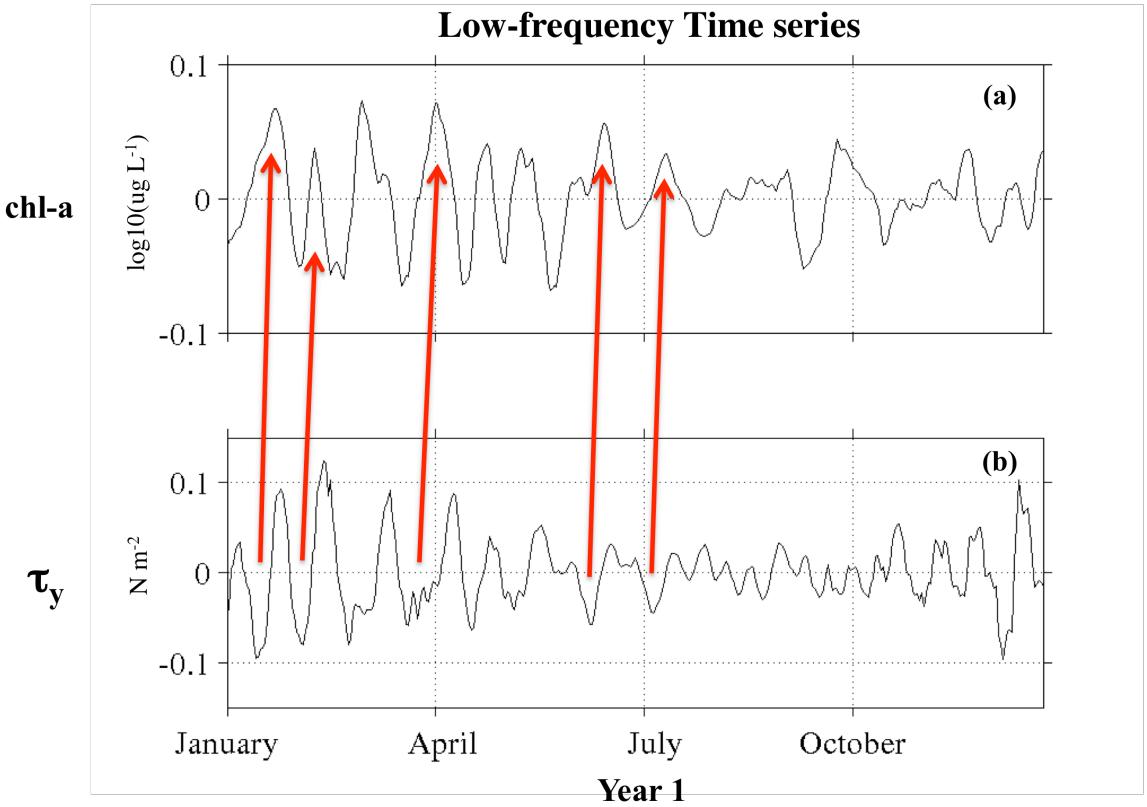

Figure 1.13: A year time series for (a) chl-a (log(ug L^{-1})) concentrations and (b) τ_y (N m^{-2}) in the CCCS (0 – 25km). The red arrows indicate the estimated lag between time series.

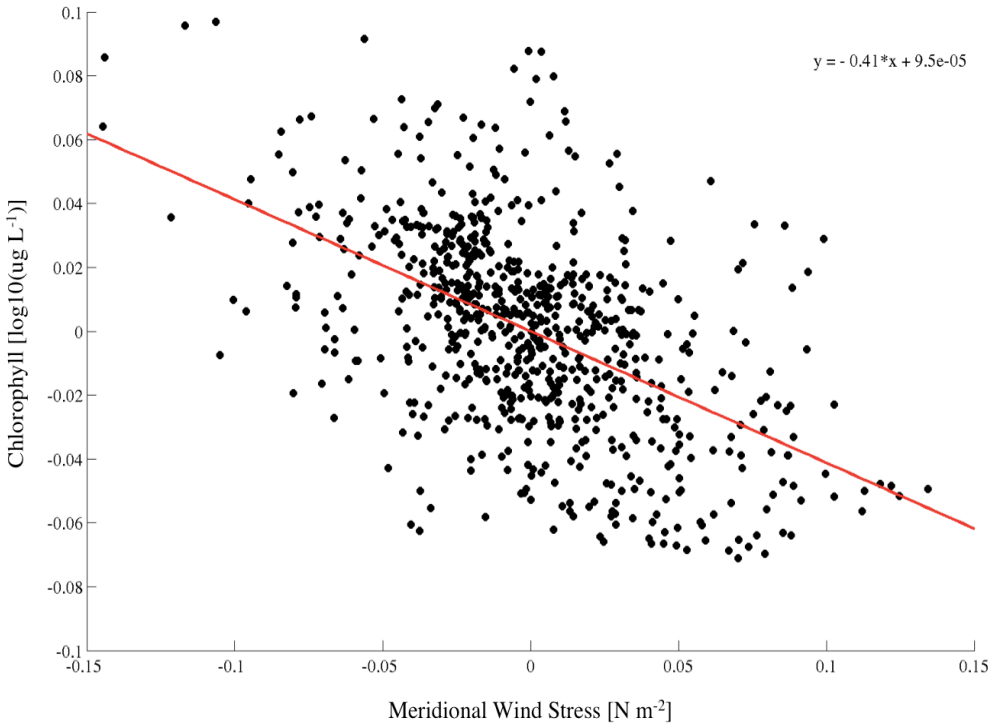

Figure 1.14: The linear relationship between chl-a (log(ug L^{-1})) and τ_y (N m^{-2}) in the CCCS (0 – 25km) at a lag of 4 days (r = -0.517; p-value << 0.0001).

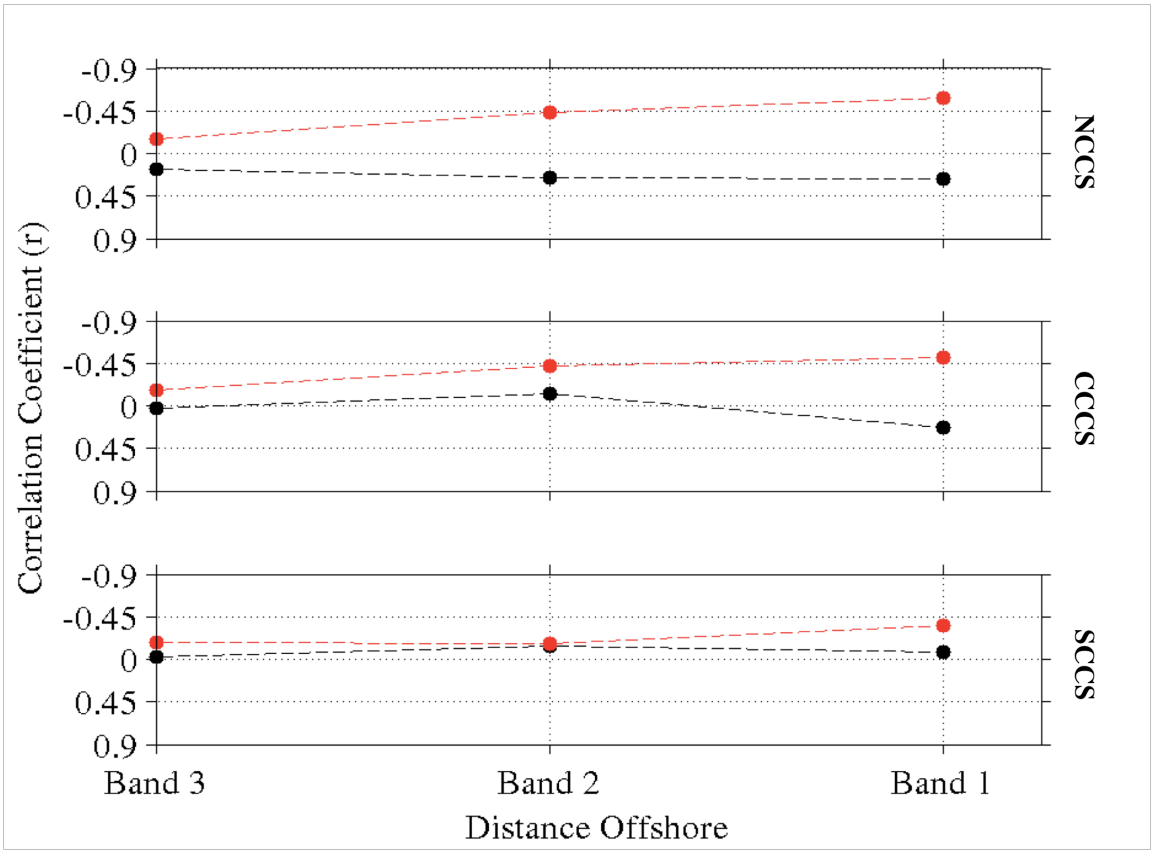

Figure 1.15: Black markers indicate correlation coefficients between the chl-a (log(ug L^{-1})) and τ_y (N m^{-2}) (2-year time series) at high frequency and red markers indicate correlations coefficients at low frequency time series within the NCCS, CCCS, and SCCS.

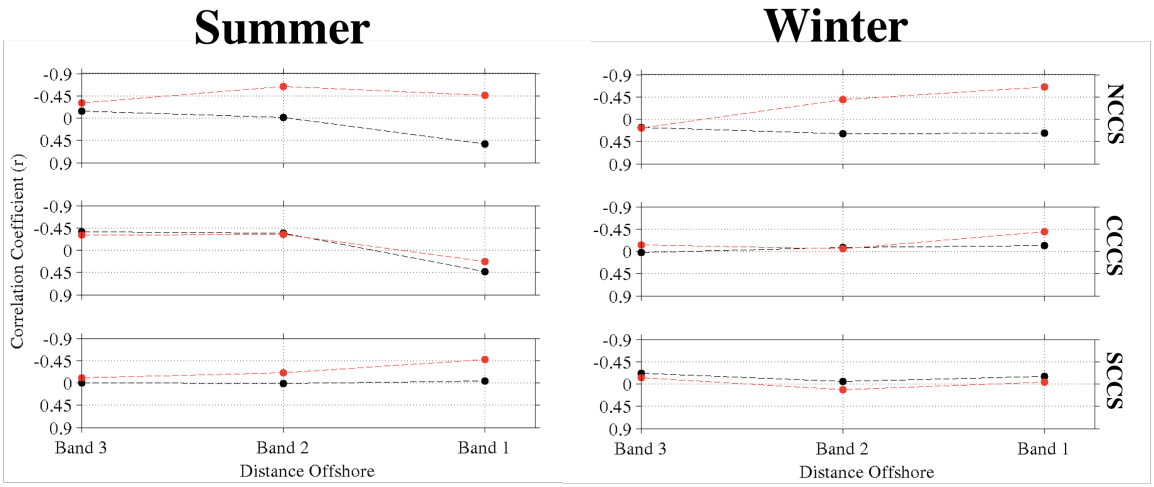

Figure 1.16: Black markers indicate correlation coefficients between chl-a (log(ug L^{-1})) and τ_y seasonal (N m^{-2}) (Summer and Winter) time series at high frequency and red markers indicate correlations coefficients at low frequency time series within the NCCS, CCCS, and SCCS.

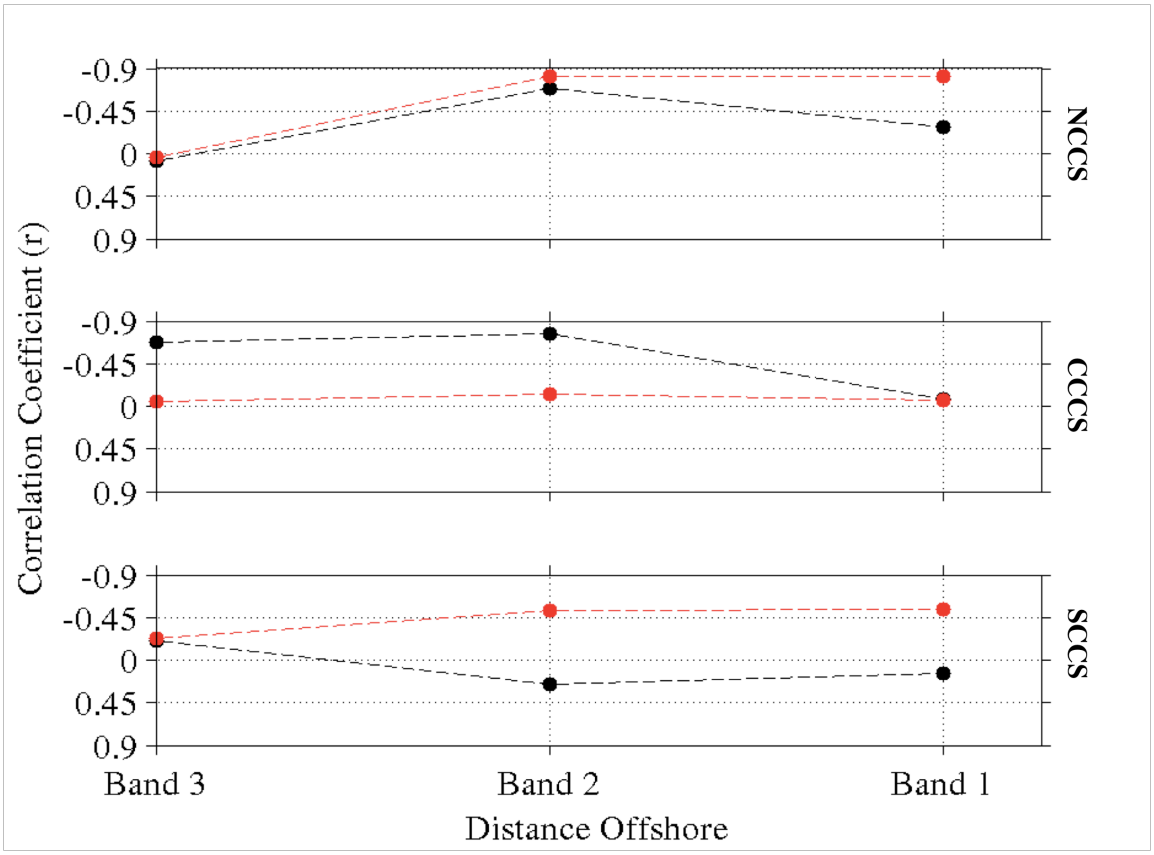

Figure 1.17: Black markers indicate correlation coefficients between nitrate (μg m^{-3}) and τ_y (N m^{-2}) seasonal (Summer) time series at high frequency and red markers indicate correlations coefficients at low frequency time series within the NCCS, CCCS, and SCCS.

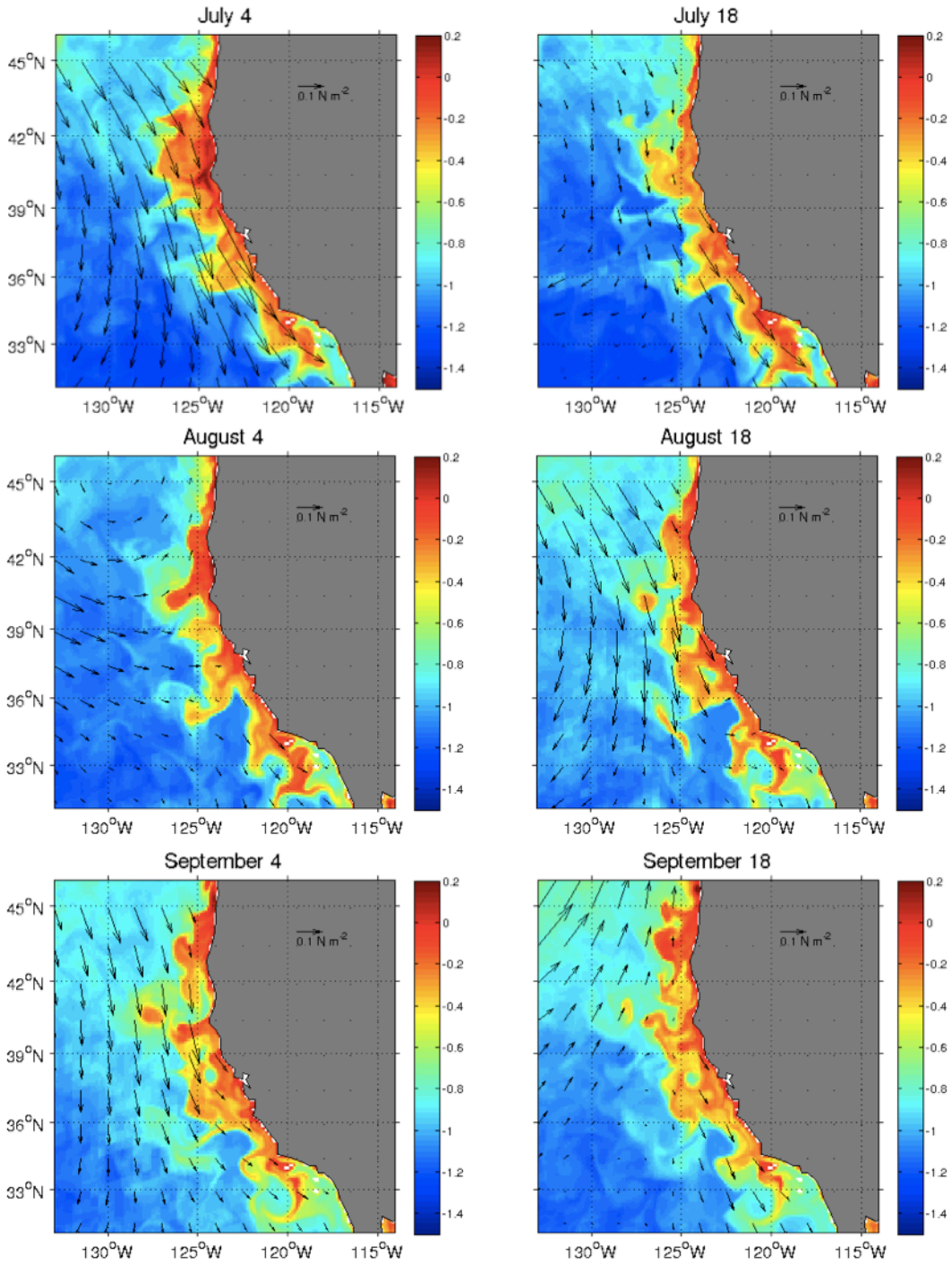

Figure 1.18: CM2.6 model Year 1: daily surface chl-a (log(ug L^{-1})) with τ_y (N m^{-2}) overlaid.

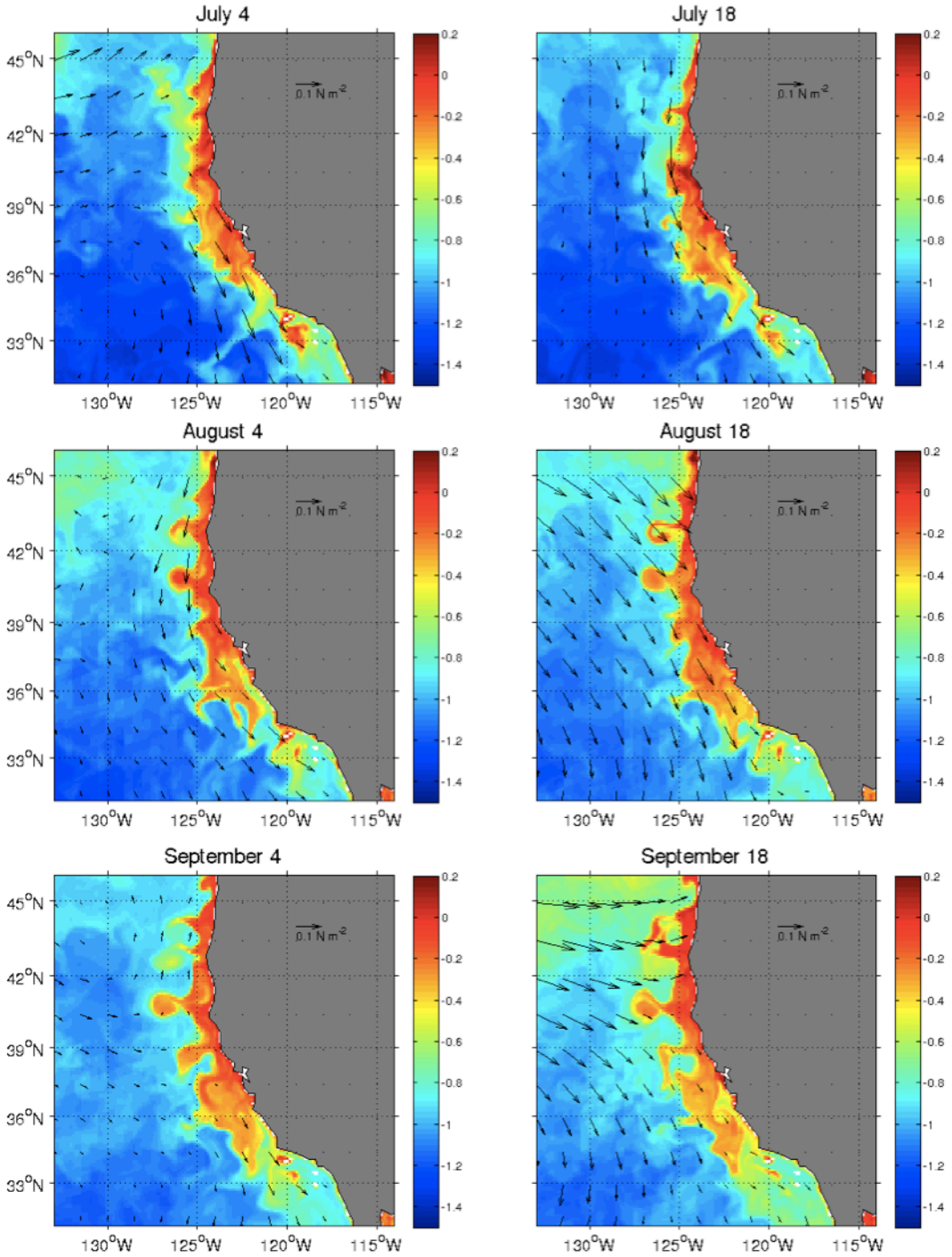

Figure 1.19: CM2.6 model Year 2: daily surface chl-a (log(ug L^{-1})) with τ_y (N m^{-2}) overlaid.

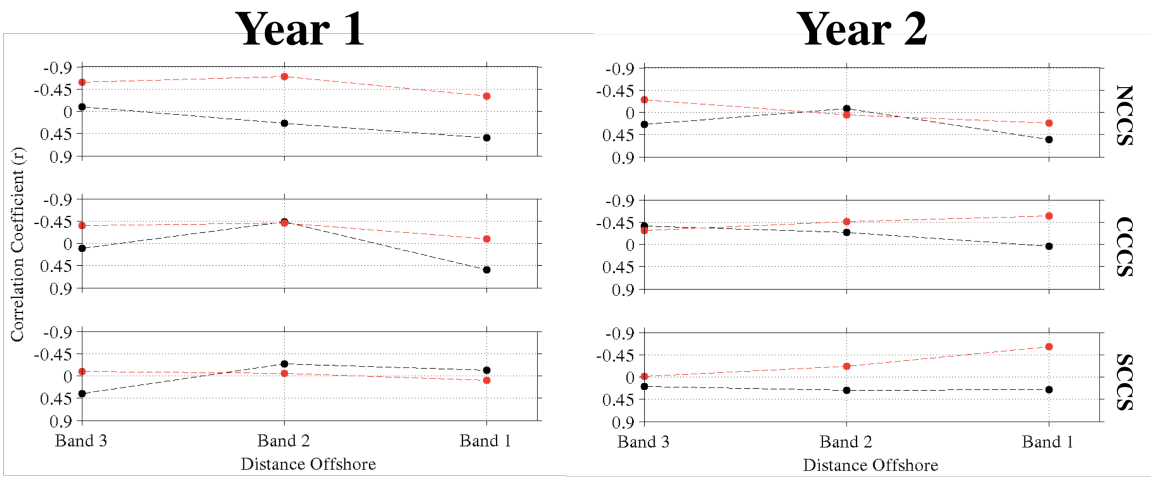

Figure 1.20: The correlation coefficients between chl-a (log(ug L^{-1})) and τ_y (N m^{-2}), at the three offshore distance ranges within the NCCS, CCCS, and SCCS, for the (a) first summer and the (b) second summer time series. Black markers indicate correlations between high frequency time series and red markers indicate correlations between low frequency time series.

REFERENCES

Abbott, M. R., and P. M. Zion (1987), Spatial and temporal variability of phytoplankton Pigment off northern California during Coastal Ocean Dynamics Experiment 1, *J. Geophy. Res.*, **92**, 1745-1756.

Agostini, V. N., A. N. Hendrix, A. B. Hollowed, C. D. Wilson, S. D. Pierce, and R. C. Francis (2008), Climate-ocean variability and Pacific hake: a geostatistical modeling approach, *J. Mar. Syst.*, **71**, 1745-1755.

Bakun, A. (1990), Global Climate Change and Intensification of Coastal Ocean Upwelling, *Science*, **247**, 198-201.

Bakun, A., D. B. Field, A. Redondo-Rodriquez, and S. J. Weeks (2010), Greenhouse gas, upwelling-favorable winds, and the future of coastal ocean upwelling ecosystems. *Glob. Chang. Biol.*, **16**, 1213-1228.

Bane, J. M., Y. H. Spitz, R. M. Letelier, and W. T. Peterson (2007), Intraseasonal oscillations in Oregon's coastal upwelling system: from the jet stream to zooplankton, *Proc. Natl. Acad. Sci. U.S.A.*, **104**, 13262-13267.

Boe, J., A. Hall, F. Colas, J. C. Williams, X. Qu, J. Kurian, and S. B. Kapnick (2011), What shapes mesoscale wind anomalies in coastal upwelling zones?, *Clim. Dyn.*, **36**, 2037-2049.

Bograd, S. J. and R. J. Lynn (2001), Physical–biological coupling in the California Current during the 1997–99 El Niño-La Niña cycle, *Geophys. Res. Lett.*, **28**, 275 278.

Botsford, L. W., C. A. Lawrence, E. P. Dever, A. Hastings, and J. Largier (2006), Effects of variable winds on biological productivity on continental shelves in coastal upwelling systems, *Deep-Sea Res. II*, **53**, 3116-3140.

Botsford, L. W., C. A. Lawrence, E. P. Dever, A. Hastings, and J. Largier (2003), Wind strength and biological productivity in upwelling systems: an idealized study, *Fish. Oceanogr.*, **12**, 245-259.

Chavez, F. P., J. Ryan, S. E. Lluch-Cota, and M. Niquen (2003), From Anchovies to Sardines and Back: Multidecadal Change in the Pacific Ocean, *Science*, **299**, 217-221.

Checkley Jr., D. M., and J. A. Barth (2009), Patterns and processes in the California Current System, *Prog. Oceanogr*, **83**, 49-64.

Chelton, D. B., P. A. Bernal, and J.A. McGowan (1982), Large-Scale Interannual Physical and Biological Interaction in the California Current, *J. Mar. Res.*, **40**, 1095-1125.

Collier, J. L., and B. Palenic (2003), Phycoerythrin-containing picoplankton in the Southern California Bight, *Deep-Sea Res. II*, **50**, 2405-2422.

Cummins, P.F., and G. S. E. Lagerloef (2004), Wind-driven interannual variability over the northeast Pacific Ocean, *Deep-Sea Res. I*, **51**, 2105-2121.

Desbiolles, F., B. Blanke, and A. Bentamy (2014), Short-term upwelling events at the western African coast related to synoptic atmospheric structures as derived from satellite observations, *J. Geophys. Res-oceans*, **119**, 461–483.

Delworth, T. L., A. Rosati, W. Anderson, A. J. Adcroft, V. Balaji, R. Benson, K. Dixon, S. M. Griffies, H. C. Lee, R. C. Pacanowski, G. A. Vecchi, A. T. Wittenberg, F. Zeng, and R. Zhang, (2012), Simulated Climate and Climate Change in the GFDL CM2.5 High-Resolution Coupled Climate Model, *J. Climate*, *25*, 2755–2781.

Demarcq, H. (2009), Trends in primary production, sea surface temperature and wind in upwelling systems (1998–2007), *Prog. Oceanogr.*, **83**, 376-385.

Di Lorenzo, E. D., A. J. Miller, D. J. Neilson, B. D. Cornuelle, and J. R. Moisan (2004), Modelling observed California Current mesoscale eddies and the ecosystem response, *Int. J. Remote Sens.*, **25**, 1307-1312.

Di Lorenzo, E., A. Miller, and N. Schneider (2005), The warming of the California Current System: Dynamics and ecosystem implications, *J. Phys. Oceanogr.*, **35**, 336–362.

Dorman, C. E., J. F. Mejia, and D. Koracin (2013), Impact of U.S. west coastline inhomogeneity and synoptic forcing on winds, wind stress, and wind stress curl during upwelling season, *J. Geophys. Res.*, **118**, 4036-4051.

Dorman, C. E., and C. D. Winant (1995), Buoy observations of the atmosphere along the west coast of the United States. 1981-1990, *J. Geophys. Res.*, **100**, 16029-16044.

Enriquez, A. G. and C. A. Friehe (1995), Effects of Wind Stress and Wind Stress Curl Variability on Coastal Upwelling, *J. Phys. Oceanogr.*, **25**, 1651-1671.

Eppley, R. W. (1972), Temperature and phytoplankton growth in the sea, *Fish B-NOAA*, 70, 1063-1085.

Freeland, H. J., G. Gatien, A. Huyer, and R. L. Smith (2003), Cold halocline in the northern California current: An inversion of subarctic water, *Geophys. Res. Lett.,* **30**, 1-4.

Garcia-Reyes, M., and J. L. Largier (2012), Seasonality of coastal upwelling off central and northern California: New insights, including temporal and spatial variability, *J. Geophys. Res.*, **117**, C03028.

Garcia-Reyes, M., and J. L. Largier (2010), Observations of increased wind-driven coastal upwelling off central California, *J. Geophys. Res.*, **115**, C04011.

García-Reyes, M., W. J. Sydeman, B. A. Black, R. R. Rykaczewski, D. S. Schoeman, S. A. Thompson, and S. J. Bograd (2013), Relative influence of oceanic and terrestrial pressure systems in driving upwelling-favorable winds, *Geophys. Res. Lett.*, **40**, 5311-5315.

GFDL Global Atmospheric Model Development Team (2004), The new GFDL global atmosphere and land model AM2-LM2: Evaluation with prescribed SST simulations. *J. Climate*, **17**, 4641-4673.

Goodman, D. R., W. Eppley, and F. M. W. Reid (1984), Summer phytoplankton assemblages and their environmental correlations in the Southern California Bight, *J. Mar. Res.*, **42**, 1019-1049.

Graham, W. M., and J. L. Largier (1997), Upwelling shadows as nearshore retention sites: the example of northern Monterey Bay. *Cont. Shelf Res.*, **17**, 509-532.

Hayward, T. L., and A. W. Mantyla (1990), Physical, chemical and biological structure of a coastal eddy near Cape Mendocino, *J. Mar. Res.*, **48**(4), 825-850.

Hickey, B., S. Geier, N. Kachel, and A. MacFadyen (2005), A bi-directional river plume: The Columbia in summer, *Cont. Shelf Res.*, **25**, 1631-1656.

Huyer, A. (1983), Coastal Upwelling in the California Current System, *Prog Oceanogr*, **12**, 259-284.

Kahru, M., R. Kudela, M. Manzano-sarabia, and B. G. Mitchell (2009), Trends in primary production in the California Current detected with satellite data, *J. Geophys. Res.*, **114**, C02004.

Kahru, M., and B. G. Mitchell (1999), Empirical chlorophyll algorithm and preliminary SeaWiFS validation for the California Current, Int. J. Remote Sens., **20**, 17, 3423-3429.

Kahru, M., and B. G. Mitchell (2001), Seasonal and nonseasonal variability of satellite

derived chlorophyll and colored dissolved organic matter concentration in the California Current, *J. Geophys. Res.*, **106**, 2517-2529.

Kelly, K. A., M. J. Caruso, J. A. Austin (1993), Wind-forced Variations in Sea Surface Height in the Northeast Pacific Ocean, *J. Phys Oceanogr.*, **23**, 2392-2411.

Kudela, R. M., N. S. Banas, J. A. Barth, E. R. Frame, D. A. Jay, J. L. Largier, E. J. Lessard, T. D. Peterson, and A. J. V. Woude (2008), New insights into the controls and mechanisms of plankton productivity in coastal upwelling waters of the northern California current system. *Oceanogr.*, **21**, 4, 46-59.

Legaard, K. R. and A. C. Thomas (2006), Spatial patterns in seasonal and interannual variability of chlorophyll and sea surface temperature in the California Current, *J. Geophys. Res.*, **111**, C06032.

Mann, K. H. (2000), Ecology of Coastal Waters, With Implications for Management, Blackwell Sci., Malden, Mass, 356-389.

Marchesiello, P., J. C. McWilliams, and A. Shcheptkin (2003), Equilibrium structure and dynamics of the California Current System, *J. Phys. Oceanogr.*, **33**(4), 753-783.

McGowan, J. A., S. J. Bograd, R. J. Lynn, and A. J. Miller (2003), The biological response to the 1977 regime shift in the California Current, *Deep-Sea Res. II*, **50**, 2567-2582.

Michaelsen, J., X. Zhang, and R. C. Smith (1988), Variability of Pigment Biomass in the California Current system as determined by Satellite Imagery 2. Temporal Variability, *J. Geophys. Res.*, **93**, 10883-10896.

Miller, C. B., and P. A. Wheeler (2012), Biological Oceanography, Wiley-Blackwell, Edition 2.

Palacios, D. M., S. J. Bograd, R. Mendelssohn, and F. B. Schwing (2004), Long-term and seasonal trends in stratification in the California Current, 1950-1993, *J. Geophys. Res.*, **109**, C10016.

Roemmich, D., and J. McGowan (1995), Climatic Warming and the Decline of Zooplankton in the California Current, *Science*, **3**, 267, 1324-1326.

Rykaczewski R. R., and D. M. Checkley, Jr (2008), Influence of ocean winds on the pelagic ecosystem in upwelling regions, *Proc. Nat. Acad. Sci.*, **105**, 1965-1970.

Schwing, F. B., S. Ralston, and K. M. Sakuma (1999), Record coastal upwelling in the California Current in 1999, *Rep. Cal. Coop. Oceanic Fish. Invest,* **41**, 148-160.

Spitz, Y. H., P. A. Newberger, and J. S. Allen (2003), Ecosystem response to upwelling off the Oregon coast: Behavior of three nitrogen-based models, *J. Geophys. Res.,* **108**, C3.

Stock, C. A., J. P. Dunne, and J. G. John (2014), Global-scale carbon and energy flows through the marine planktonic food web: An analysis with a coupled physical biological model, *Prog. Oceanogr.*, **120**, 1-28.

Strub, P. T., J. S. Allen, A. Huyer, R. L. Smith, and R. C. Beardsley (1987a), Seasonal cycles of currents, temperatures, winds, and sea level over the northeast Pacific continental shelf: 35°N to 48°N, *J. Geophys. Res.*, **92**, 1507-1526.

Strub, P. T., J. S. Allen, A. Huyer, and R. L. Smith (1987b), Large-scale structure of the spring transition in the coastal ocean off western North America, *J. Geophys. Res.*, **92**, 1527-1544.

Strub, P. T., and C. James (2003), Altimeter estimates of anomalous transports into the northern California Current during 2000-2002, *Geophys. Res. Lett.*, **30**, 8025, 1-4.

Strub, P. T., C. James, A. C. Thomas, and M. R. Abbott (1990), Seasonal and nonseasonal variability of satellite-derived surface pigment concentration in the California Current, *J. Geophys. Res.*, **95**(C7), 11501–11530.

Strub, P. T., P. M. Kosro, an A. Huyer (1991), The Nature of the Cold Filaments in the California Current System, *J. Geophys. Res.*, **96**(C8), 14743-14768.

Thomas, A. C., F. Huang, P. Ted Strub, and C. James (1994), Comparison of the seasonal and interannual variability of phytoplankton pigment concentrations in the Peru and California Current systems. *J. Geophys. Res*, **99**(C4) 7355-7370.

Thomas, A. C., and Weatherbee, R. A. (2006), Satellite-measured temporal variability of the Columbia River plume, *Remote Sens. Environ.*, **100**, 2, 167-178.

Venrick, E. L. (2002), Floral patterns in the California current system off southern California: 1990-1996, *J. Mar. Res.*, **60**, 171-189.

Weeks, S. J., R. Barlow, C. Roy, and F. A. Shillington (2006), Remotely sensed variability of temperature and chlorophyll in the southern Benguela: upwelling frequency and phytoplankton response, *Afri. J. Mar. Sci.*, **28**, 3-4.

Wessel, P., and W. H. F. Smith (1996), A Global Self-consistent, Hierarchical, High resolution Shoreline Database, *J. Geophys. Res.*, **101**, 8741-8743.

Winton, M., W. G. Anderson, T. L. Delworth, S. M. Griffies, W. J. Hurlin, and A. Rosati (2014), Has coarse ocean resolution biased simulations of transient climate sensitivity?, *Geophys. Res. Lett.*, **41**, 1-8.

Wroblewski, J. S., J. G. Richman, and G. L. Mellor (1989), Optimal Wind Conditions for the Survival of Larval Northern Anchovy, *Engraulis mordax*: A Modeling Study, *Fish. Bull.*, **87**, 387-395.

Zhang, H.-M., J.J. Bates, and R.W. Reynolds (2006), Assessment of composite global sampling: Sea surface wind speed, *Geophys. Res. Lett.,* **33**, L17714.